This is a preprint of: "Topological Classification of Quadratic Polynomial Differential Systems with a Finite Semi-Elemental Triple Saddle", Joan Carles Artés, Regilene D. S. Oliveira, Alex Carlucci Rezende, *Internat. J. Bifur. Chaos Appl. Sci. Engrg.*, vol. 26(11), 1650188 (26 pages), 2016.
DOI: [10.1142/S0218127416501881]

TOPOLOGICAL CLASSIFICATION OF QUADRATIC POLYNOMIAL DIFFERENTIAL SYSTEMS WITH A FINITE SEMI–ELEMENTAL TRIPLE SADDLE

JOAN C. ARTÉS
Departament de Matemàtiques, Universitat Autònoma de Barcelona, 08193 Bellaterra, Barcelona, Spain
E–mail: artes@mat.uab.cat

REGILENE D. S. OLIVEIRA
Departamento de Matemática, Universidade de São Paulo, 13566–590, São Carlos, São Paulo, Brazil,
E–mail: regilene@icmc.usp.br

ALEX C. REZENDE
Departament de Matemàtiques, Universitat Autònoma de Barcelona, 08193 Bellaterra, Barcelona, Spain
E–mail: alexcrezende@gmail.com

The study of planar quadratic differential systems is very important not only because they appear in many areas of applied mathematics but due to their richness in structure, stability and questions concerning limit cycles, for example. Even though many papers have been written on this class of systems, a complete understanding of this family is still missing. Classical problems, and in particular Hilbert's 16th problem [Hilbert, 1900, Hilbert, 1902], are still open for this family. In this article we make a global study of the family $\mathbf{QT\overline{S}}$ of all real quadratic polynomial differential systems which have a finite semi–elemental triple saddle (triple saddle with exactly one zero eigenvalue). This family modulo the action of the affine group and time homotheties is three–dimensional and we give its bifurcation diagram with respect to a normal form, in the three–dimensional real space of the parameters of this normal form. This bifurcation diagram yields 27 phase portraits for systems in $\mathbf{QT\overline{S}}$ counting phase portraits with and without limit cycles. Algebraic invariants are used to construct the bifurcation set and we present the phase portraits on the Poincaré disk. The bifurcation set is not only algebraic due to the presence of a surface found numerically, whose points correspond to connections of separatrices.

1. Introduction, brief review of the literature and statement of the results

We call *quadratic differential systems* or simply *quadratic systems*, differential systems of the form

$$\dot{x} = p(x, y), \quad \dot{y} = q(x, y), \tag{1}$$

where p and q are polynomials over $\mathbb{R}$ in x and y such that the $\max(\deg(p),\deg(q)) = 2$. We can always associate to such a system the quadratic vector field

$$\xi = p\,\frac{\partial}{\partial x} + q\,\frac{\partial}{\partial y}, \tag{2}$$

as well as the differential equation

$$q\,dx - p\,dy = 0. \tag{3}$$

The class of all quadratic differential systems (or quadratic vector fields) will be denoted by **QS**.

We can also write system (1) as

$$\begin{aligned} \dot{x} &= p_0 + p_1(x, y) + p_2(x, y) = p(x, y),\\ \dot{y} &= q_0 + q_1(x, y) + q_2(x, y) = q(x, y), \end{aligned} \tag{4}$$

where p_i and q_i are homogeneous polynomials of degree i in the variable (x, y) with real coefficients with $p_2^2 + q_2^2 \neq 0$.

A complete classification of the phase portraits of real planar quadratic differential systems is still not known, even after hundreds of papers on their topology, and attempting to topologically classify them is considerably a complicated task. This family of systems is subjected to twelve parameters, but after the action of the group $\mathrm{Aff}(2, \mathbb{R})$ of real affine transformations and time homotheties, the class lastly depends on five parameters, which is still a large number.

The main goal of this paper is to study the class $\mathbf{QT\overline{S}}$ of all quadratic systems possessing a finite semi–elemental triple saddle, and then contribute to the analysis of the quadratic systems possessing finite semi–elemental singular points initiated with the articles by Artés, Rezende and Oliveira dealing with finite semi–elemental triple node [Artés *et al.*, 2013] and finite semi–elemental saddle–node [Artés *et al.*, 2014, Artés *et al.*, 2015b]. A semi–elemental singular point is a singularity with zero determinant of its Jacobian, but with only one eigenvalue zero. This such a point is known in classical literature as semi–elementary, but we use the term semi–elemental introduced in [Artés *et al.*, 2015a] as part of a set of new definitions more deeply related to singular points, their multiplicities and, specially, their Jacobian matrices.

Besides the finite triple saddle $\bar{s}_{(3)}$, systems in $\mathbf{QT\overline{S}}$ could have another finite singular point. Indeed, in case the remaining singularity did not go to infinity, then there is one more singularity in the finite plane, or even the origin may have higher multiplicity.

For a general framework of the study of the class of all quadratic differential systems we refer to the article of Roussarie and Schlomiuk [Roussarie & Schlomiuk, 2002].

In the present analysis we follow the pattern set out in [Artés *et al.*, 2006] and, in order to avoid repeating technical sections which are the same for both papers, we refer to the paper mentioned for more complete information.

We now give the notion of *graphics*, which play an important role in obtaining limit cycles when they are due to connection of separatrices, for example.

A *(non-degenerate) graphic* as defined in [Dumortier *et al.*, 1994] is formed by a finite sequence of singular points $r_1, r_2, \ldots, r_n$ (with possible repetitions) and non–trivial connecting orbits γ_i for $i = 1, \ldots, n$ such that γ_i has r_i as α–limit set and r_{i+1} as ω–limit set for $i < n$ and γ_n has r_n as α–limit set and r_1 as ω–limit set. Also normal orientations n_j of the non–trivial orbits must be coherent in the sense that if γ_{j-1} has left–hand orientation then so does γ_j. A *polycycle* is a graphic which has a Poincaré return map.

A *degenerate graphic* is formed by a finite sequence of singular points $r_1, r_2, \ldots, r_n$ (with possible repetitions) and non–trivial connecting orbits and/or segments of curves of singular points γ_i for $i = 1, \ldots, n$ such that γ_i has r_i as α–limit set and r_{i+1} as ω–limit set for $i < n$ and γ_n has r_n as α–limit set and r_1 as ω–limit set. Also normal orientations n_j of the non–trivial orbits must be coherent in the sense that if γ_{j-1} has left–hand orientation then so does γ_j. For more details, see [Dumortier *et al.*, 1994].

In [Artés *et al.*, 1998] the authors analyzed the structurally stable quadratic planar systems

and they proved the existence of 44 topologically distinct phase portraits for this family, modulo limit cycles. These systems are also known as the codimension–zero quadratic systems. Roughly speaking, these systems are characterized by having only simple finite and infinite singularities, no separatrix connection, and where any nest of limit cycles is considered as a single point with the stability of the outer limit cycle.

The intention now is to classify the structurally unstable quadratic systems of codimension–one which have one, and only one, of the simplest structurally unstable objects: a saddle–node of multiplicity two (finite or infinite), a separatrix from one saddle point to another, and a separatrix forming a loop for a saddle point with its divergence nonzero. In accordance to what is described in [**?**], all the codimension–one phase portraits are split into four groups according to the possession of a structurally unstable element: (A) possessing a finite semi–elemental saddle–node $\overline{sn}_{(2)}$, (B) possessing an infinite semi–elemental saddle–node $\binom{\overline{0}}{2}SN$, (C) possessing an infinite semi–elemental saddle–node $\binom{\overline{1}}{1}SN$, and (D) possessing a saddle connection.

The study of the codimension–one systems is already in progress [Artés *et al.*, 2016]. All the topological possibilities have already been found, some of them have already been proved impossible and many representatives have been found, but few cases without candidate still remain. A way to obtain phase portraits of codimension one is applying perturbation in phase portraits of quadratic systems of higher codimension already known. This perturbation may decrease the codimension of the system and a representative for a topological equivalence class in the family of the codimension–one systems may be found and added to the existing classification.

With the purpose of furnishing with this classification, some families of quadratic systems of codimension greater than one have been analyzed, e.g. systems with a weak focus of second order (see [Artés *et al.*, 2006]), with a finite semi–elemental triple node (see [Artés *et al.*, 2013]) and the family possessing saddle–nodes (see [Artés *et al.*, 2014, Artés *et al.*, 2015b]). It is worth mentioning that in [Artés *et al.*, 2013, Artés *et al.*, 2014, Artés *et al.*, 2015b], the authors show that, after a quadratic perturbation of one of the phase portraits of those families, all the codimension–one phase portraits from group (A) are proved being realizable, as well as some phase portraits from group (B).

The present study is part of this attempt of classifying all the codimension–one quadratic systems. Although we could not find any remaining case from group (B), this study contributes to the classification of the quadratic systems with finite semi–elemental singular points.

All these classifications of codimension–two families are also of great value since once finished the complete set of structurally unstable phase portraits of codimension one, modulo limit cycles, we plan to afford the codimension two in which the generic cases of these families will be the most needed items.

In the normal form (7), the class $\mathbf{QT\overline{S}}$ is divided into 71 parts: 16 three–dimensional ones, 31 two–dimensional ones, 19 one–dimensional ones and 5 points. This partition is obtained by considering all the bifurcation surfaces of singularities and one related to connections of separatrices, modulo "islands" (see Sec. 7).

We observe that this partition and the number of topological phase portraits for this family depend on the choice of the specific normal form (7). According to [Schlomiuk, 2014], this partition does not necessarily contain all the phase portraits of the closure within the quadratic differential systems. It is possible that given two different normal forms for the same family, one phase portrait may exist in the closure of one of them but not in the closure of the other. However, the interior of the family in any normal form must contain exactly the same phase portraits.

Theorem 1.1. *There exist 27 distinct phase portraits for the quadratic vector fields having a finite semi–elemental triple saddle. All these phase portraits are shown in Fig. 1. Moreover, the following statements hold:*

(a) There exist four phase portraits with limit cycles, and they are in the regions V_8, V_9, $5S_6$ *and* $5S_7$*;*

(b) There exist five phase portraits with graphics, and they are in the regions $7S_1$, $7S_2$, $1.3L_1$, $5.7L_1$ *and* $5.7L_2$*.*

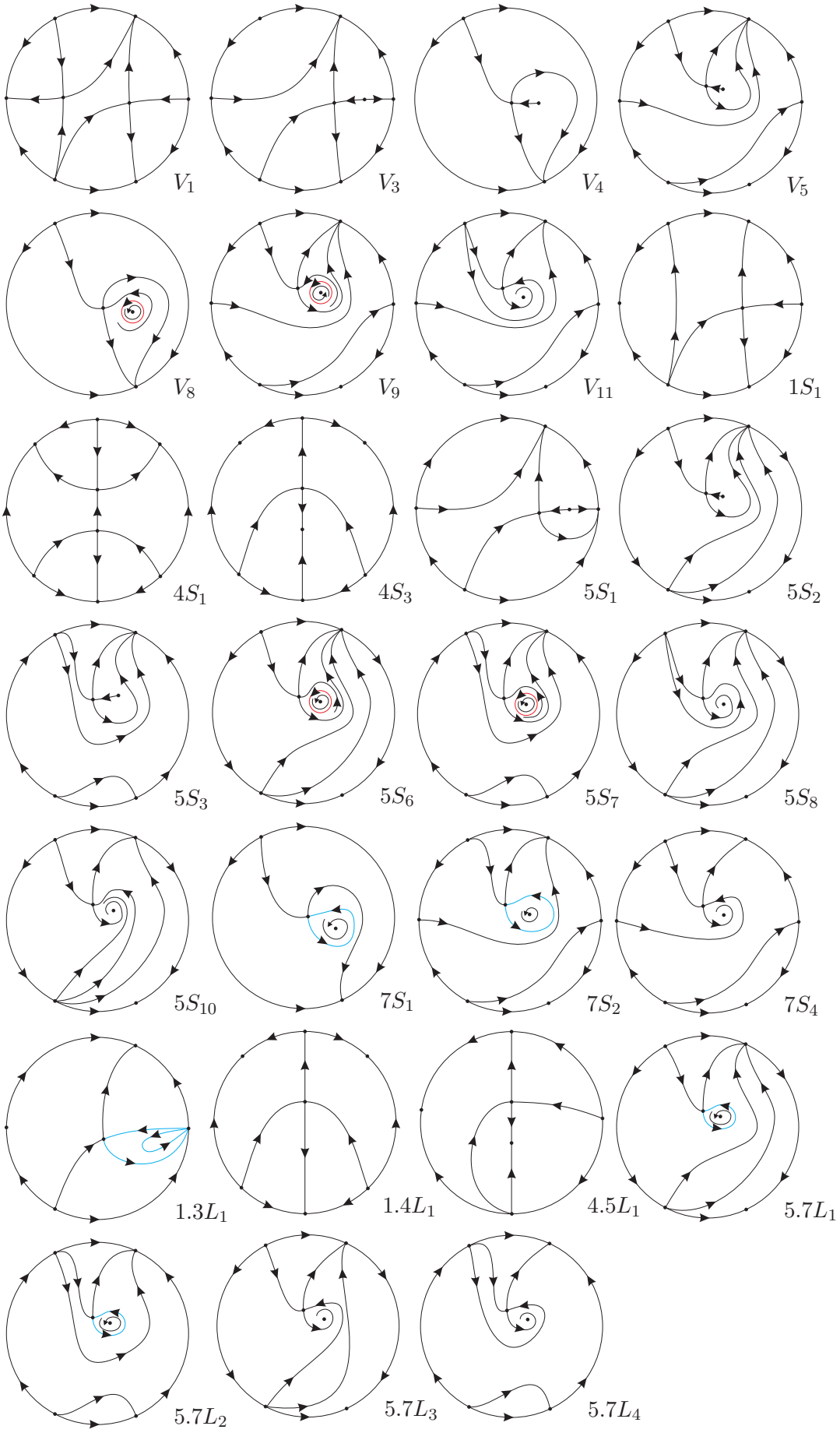

Fig. 1. Phase portraits for quadratic vector fields with a finite semi–elemental triple saddle

From the 27 different phase portraits, 7 occur in 3–dimensional parts, 13 in 2–dimensional parts and 7 in 1–dimensional parts.

In Fig. 1 we have denoted with a little disk the singular points and we have plotted with wide curves the separatrices and we have added some thinner orbits in few required cases to avoid confusion.

Remark 1.2. We label the phase portraits according to the parts of the bifurcation diagram where they occur. These labels could be different for two topologically equivalent phase portraits occurring in distinct parts. Some of the phase portraits in 3–dimensional parts also occur in some lower dimensional parts bordering these 3–dimensional parts. An example occurs when a node turns into a focus. An analogous situation happens for phase portraits in 2–dimensional or 1–dimensional parts, coinciding with a phase portrait situated on their border.

This paper is organized as follows. In Sec. 2 we describe the normal form for the family of systems having a finite semi–elemental triple saddle.

In Sec. 3 we describe very succinctly the Poincaré compactification on the 2–dimensional sphere, which is used to draw the global phase portraits.

Sec. 4 presents a list of some very basic properties of general quadratic systems needed in this study.

In Sec. 5 we mention some algebraic and geometric concepts that were introduced in [Schlomiuk & Pal, 2001, Llibre & Schlomiuk, 2004] involving intersection numbers, zero–cycles, divisors, and T–comitants and invariants for quadratic systems as used by the Sibirskii school. We refer the reader directly to [Artés *et al.*, 2006] where these concepts are widely explained.

In Sec. 6, using algebraic invariants and T–comitants, we construct the bifurcation surfaces for the class $\mathbf{QT\overline{S}}$.

In Sec. 7 we describe the possible (but unfounded yet) existence of "islands".

In Sec. 8 we introduce a global invariant denoted by $\mathcal{I}$, which classifies completely, up to topological equivalence, the phase portraits we have obtained for the systems in the class $\mathbf{QT\overline{S}}$. Theorem 8.7 shows clearly that they are uniquely determined (up to topological equivalence) by the values of the invariant $\mathcal{I}$.

2. Quadratic vector fields with a finite semi–elemental triple saddle

A singular point r of a planar vector field ξ in $\mathbb{R}^2$ is *semi–elemental* if the determinant of the matrix of its linear part, $D\xi(r)$, is zero, but its trace is different from zero.

The following result by Andronov *et al.* [Andronov *et al.*, 1973], and also found in [Dumortier *et al.*, 2006], characterizes the local phase portrait at a finite semi–elemental singular point.

Proposition 2.1. *Let $r = (0, 0)$ be an isolated singular point of the vector field ξ given by*

$$\dot{x} = A(x, y), \quad \dot{y} = y + B(x, y), \tag{5}$$

where A and B are analytic in a neighborhood of the origin starting with a degree at least 2 in the variables x and y. Let $y = f(x)$ be the solution of the equation $y + B(x, y) = 0$ in a neighborhood of the point $r = (0, 0)$, and suppose that the function $g(x) = A(x, f(x))$ has the expression $g(x) = ax^\alpha + o(x^\alpha)$, where $\alpha \geq 2$ and $a \neq 0$. So, when α is odd, then $r = (0, 0)$ is either an unstable multiple node, or a multiple saddle, depending if $a > 0$, or $a < 0$, respectively. In the case of the multiple saddle, the separatrices are tangent to the x–axis. If α is even, the $r = (0, 0)$ is a multiple saddle–node, i.e. the singular point is formed by the union of two hyperbolic sectors with one parabolic sector. The stable separatrix is tangent to the positive (respectively, negative) x–axis at $r = (0, 0)$ according to $a < 0$ (respectively, $a > 0$). The two unstable separatrices are tangent to the y–axis at $r = (0, 0)$.

In the particular case where A and B are real quadratic polynomials in the variables x and y, a quadratic system with a finite semi–elemental singular point at the origin can always be written into the form

$$\begin{aligned} \dot{x} &= gx^2 + 2hxy + ky^2, \\ \dot{y} &= y + \ell x^2 + 2mxy + ny^2. \end{aligned} \tag{6}$$

Applying Proposition 2.1 to system (6), we conclude that, if $g \neq 0$, then the origin is a double

semi–elemental saddle–node $\overline{sn}_{(2)}$ and, if $g = 0$ and $h\ell \neq 0$, then the origin is a semi–elemental triple node $\bar{n}_{(3)}$, if $\ell < 0$, and it is a semi–elemental triple saddle $\bar{s}_{(3)}$, if $\ell > 0$.

In the normal form (6), we consider the coefficient of the terms xy in both equations multiplied by 2 in order to make easier the calculations of the algebraic invariants we shall compute later.

The following result states the normal form for systems in $\mathbf{QT\overline{S}}$.

Proposition 2.2. *Every planar quadratic system with a finite semi–elemental triple saddle $\bar{s}_{(3)}$ can be brought via affine transformations and time rescaling to the following normal form:*

$$\begin{aligned} \dot{x} &= 2xy + ky^2, \\ \dot{y} &= y + x^2 + 2mxy + ny^2, \end{aligned} \tag{7}$$

where k, m and n are real parameters.

Proof. We start with system (6). By Proposition 2.1, we set $g = 0$ and $h\ell \neq 0$ in order to have a semi–elemental triple point at the origin. Since the function $g(x) = -2h\ell x^3 + o(x^4)$ starts with odd degree, it implies that the triple point is either a node or a saddle. If $-2h\ell < 0$, we shall have a triple saddle. Since $h\ell \neq 0$, after the affine transformation $(x, y) \mapsto (\sqrt{h\ell}x, hy)$, we can fix $h = 1$ and then $\ell = 1$, completing the proof. ∎

Since the normal form (7) depends on the real coefficients k, m and n, the parameter space is $\mathbb{R}^3$ with coordinates (m, n, k). We shall foliate this parameter space $\mathbb{R}^3$ in the variable k.

Remark 2.3. After rescaling the time, we note that system (7) is symmetric in relation to the real parameter k. So, we will only consider $k \geq 0$.

3. The Poincaré compactification and the complex (real) foliation with singularities on $\mathbb{CP}^2$ ($\mathbb{RP}^2$)

A real planar polynomial vector field ξ can be compactified on the sphere as follows. Consider the $xy-$plane as being the plane $Z = 1$ in the space $\mathbb{R}^3$ with coordinates X, Y and Z. The central projection of the vector field ξ on the sphere of radius one yields a diffeomorphic vector field on the both upper and lower hemispheres. There exists an analytic vector field $cp(\xi)$ on the whole sphere such that its restriction on the upper hemisphere has the same phase curves as the one constructed above from the polynomial vector field (for a proof see [Gonzales, 1969]). The projection of the closed northern hemisphere H^+ of $\mathbb{S}^2$ on $Z = 0$ under $(X, Y, Z) \mapsto (X, Y)$ is called *the Poincaré disk*. A singular point q of $cp(\xi)$ is called an *infinite* (respectively, *finite*) singular point if $q \in \mathbb{S}^1$ (respectively, $q \in \mathbb{S}^2 \setminus \mathbb{S}^1$). We call the circle $\mathbb{S}^1$ by the equator of the sphere $\mathbb{S}^2$. By the *Poincaré compactification of a polynomial vector field* we mean the vector field $cp(\xi)$ restricted to the upper hemisphere completed with the equator.

We now drive our attention to Darboux's ideas [Darboux, 1878] in the remaining part of this section. Let $p(x, y)$ and $q(x, y)$ be polynomials with real coefficients. For the vector field

$$p\,\frac{\partial}{\partial x} + q\,\frac{\partial}{\partial y}, \tag{8}$$

or, equivalently, for the differential system

$$\dot{x} = p(x, y), \qquad \dot{y} = q(x, y), \tag{9}$$

we consider the associated differential 1–form $\omega_1 = q(x, y)\,dx - p(x, y)\,dy$, and the differential equation

$$\omega_1 = 0. \tag{10}$$

Clearly, equation (10) defines a foliation with singularities on $\mathbb{C}^2$. The affine plane $\mathbb{C}^2$ is compactified on the complex projective space $\mathbb{CP}^2 = (\mathbb{C}^3 \setminus \{0\})/\sim$, where $(X, Y, Z) \sim (X', Y', Z')$ if, and only if, $(X, Y, Z) = \lambda(X', Y', Z')$, for some complex $\lambda \neq 0$. The equivalence class of (X, Y, Z) will be denoted by $[X : Y : Z]$.

The foliation with singularities defined by equation (10) on $\mathbb{C}^2$ can be extended to a foliation with singularities on $\mathbb{CP}^2$ and the $1-$form ω_1 can be extended to a meromorphic $1-$form ω on $\mathbb{CP}^2$ which yields an equation $\omega = 0$, i.e.

$$A(X, Y, Z)dX + B(X, Y, Z)dY + C(X, Y, Z)dZ = 0, \tag{11}$$

whose coefficients A, B, C are homogeneous polynomials of the same degree and satisfy the relation:

$$A(X, Y, Z)X + B(X, Y, Z)Y + C(X, Y, Z)Z = 0. \tag{12}$$

Indeed, consider the map $i : \mathbb{C}^3 \setminus \{Z = 0\} \to \mathbb{C}^2$, given by $i(X, Y, Z) = (X/Z, Y/Z) = (x, y)$ and suppose that $\max(\deg(p), \deg(q)) = m > 0$. Since $x = X/Z$ and $y = Y/Z$, we have:

$$dx = (ZdX - XdZ)/Z^2, \quad dy = (ZdY - YdZ)/Z^2,$$

the pull–back form $i^*(\omega_1)$ has poles at $Z = 0$ and yields the equation

$$\begin{aligned} i^*(\omega_1) =& q(X/Z, Y/Z)(ZdX - XdZ)/Z^2 \\ & - p(X/Z, Y/Z)(ZdY - YdZ)/Z^2 = 0. \end{aligned}$$

Then, the 1−form $\omega = Z^{m+2} i^*(\omega_1)$ in $\mathbb{C}^3 \setminus \{Z \neq 0\}$ has homogeneous polynomial coefficients of degree $m + 1$, and for $Z = 0$ the equations $\omega = 0$ and $i^*(\omega_1) = 0$ have the same solutions. Therefore, the differential equation $\omega = 0$ can be written as (11), where

$$\begin{aligned} A =& ZQ(X, Y, Z) = Z^{m+1} q(X/Z, Y/Z), \\ B =& - ZP(X, Y, Z) = -Z^{m+1} p(X/Z, Y/Z), \\ C =& YP(X, Y, Z) - XQ(X, Y, Z) = \\ =& Z^m (Yp(X/Z, Y/Z) - Xq(X/Z, Y/Z)). \end{aligned} \tag{13}$$

Clearly A, B and C are homogeneous polynomials of degree $m + 1$ satisfying (12).

In particular, for our quadratic systems (7), A, B and C take the following forms

$$\begin{aligned} A(X, Y, Z) =& Z(X^2 + 2mXY + nY^2 + YZ), \\ B(X, Y, Z) =& - YZ(2X + kY), \\ C(X, Y, Z) =& - X^3 - 2mX^2Y + 2XY^2 \\ & - nXY^2 + kY^3 - XYZ. \end{aligned} \tag{14}$$

We note that the straight line $Z = 0$ is always an algebraic invariant curve of this foliation and that its singular points are the solutions of the system: $A(X, Y, Z) = B(X, Y, Z) = C(X, Y, Z) = 0$.

To study the foliation with singularities defined by the differential equation (11) subject to (12) with A, B and C satisfying the above conditions in the neighborhood of the line $Z = 0$, we consider the two charts of $\mathbb{CP}^2$: $(u, z) = (Y/X, Z/X)$, $X \neq 0$, and $(v, w) = (X/Y, Z/Y)$, $Y \neq 0$, covering this line. We note that in the intersection of the charts $(x, y) = (X/Z, Y/Z)$ and (u, z) (respectively, (v, w)) we have the change of coordinates $x = 1/z$, $y = u/z$ (respectively, $x = v/w$, $y = 1/w$). Except for the point $[0 : 1 : 0]$ or the point $[1 : 0 : 0]$, the foliation defined by equations (11) and (12) with A, B and C as in (13) yields in the neighborhood of the line $Z = 0$ the foliations associated with the systems

$$\begin{aligned} \dot{u} =& uP(1, u, z) - Q(1, u, z) = C(1, u, z), \\ \dot{z} =& zP(1, u, z), \end{aligned} \tag{15}$$

or

$$\begin{aligned} \dot{v} =& vQ(v, 1, w) - P(v, 1, w) = -C(v, 1, w), \\ \dot{w} =& wP(v, 1, w). \end{aligned} \tag{16}$$

In a similar way we can associate a real foliation with singularities on $\mathbb{RP}^2$ to a real planar polynomial vector field.

4. A few basic properties of quadratic systems relevant for this study

We list below results involving any quadratic system which, in particular, play an important role in the study of the global phase portraits of the real planar quadratic systems (1) having a semi–elemental triple saddle.

(i) A straight line either has at most two (finite) contact points with a quadratic system (which include the singular points), or it is formed by trajectories of the system; see Lemma 11.1 of [Ye *et al.*, 1986]. We recall that by definition a *contact point* of a straight line L is a point of L where the vector field has the same direction as L, or it is zero.

(ii) If a straight line passing through two real finite singular points r_1 and r_2 of a quadratic system is not formed by trajectories, then it is divided by these two singular points in three segments $\overline{\infty r_1}$, $\overline{r_1 r_2}$ and $\overline{r_2 \infty}$ such that the trajectories cross $\overline{\infty r_1}$ and $\overline{r_2 \infty}$ in one direction, and they cross $\overline{r_1 r_2}$ in the opposite direction; see Lemma 11.4 of [Ye *et al.*, 1986].

(iii) If a quadratic system has a limit cycle, then it surrounds a unique singular point, and this point is a focus; see [Coppel, 1966].

Proposition 4.1. *The border of any simply connected closed bidimensional set which is invariant under the flow of a vector field must either*

1) surround a singular point of index greater than or equal to +1, or

2) contain a singular point having an elliptic sector situated in the region delimited by the border, or

3) contain or surround an infinite number of singular points.

For a proof of Proposition 4.1 see [Artés *et al.*, 1998] or [Artés *et al.*, 2013].

5. Some algebraic and geometric concepts

In this article we use the concept of intersection number for curves (see [Fulton, 1969]). For a quick summary see Sec. 5 of [Artés *et al.*, 2006].

We shall also use the concepts of zero–cycle and divisor (see [Hartshorne, 1977]) as specified for quadratic vector fields in [Schlomiuk & Pal, 2001]. For a quick summary see Sec. 6 of [Artés *et al.*, 2006].

We shall also use the concepts of algebraic invariant and T–comitant as used by the Sibirskii school for differential equations. For a quick summary see Sec. 7 of [Artés *et al.*, 2006].

6. The bifurcation diagram of the systems with a finite semi–elemental triple saddle

We recall that, since the normal form (7) involves the real coefficients m, n and k, the parameter space is $\mathbb{R}^3$ with coordinates (m, n, k).

In what follows we describe all the bifurcation surfaces which are necessary to construct the bifurcation diagram. Regarding the definition of the invariants and T–comitants (we refer to Sec. 5), these surfaces are described by the set of zeroes of such T–comitants and invariants. These are polynomials in the coefficients of system (7) and possibly in the variables x and y.

6.1. Bifurcation surfaces due to the changes in the nature of singularities

The origin for the normal form (7) is a semi–elemental triple saddle.

The formulas which provide the bifurcation surfaces of singularities in $\mathbb{R}^{12}$, produced by changes that may occur in the local nature of finite singularities are given in Sec. 7 of [Artés *et al.*, 2008]. Equivalently, in [Schlomiuk & Vulpe, 2005] we obtain such formulas for the infinite singular points. These bifurcation surfaces are all algebraic and they are the following:

Bifurcation surfaces in $\mathbb{R}^3$ due to multiplicities of singularities

$(\mathcal{S}_1)$ This is the bifurcation surface due to multiplicity of infinite singularities involved with finite singular points. This occurs when at least one finite singular point coalesces with at least one infinite singular point. This is a conic whose equation is

$$\mu = k^2 - 4km + 4n = 0.$$

$(\mathcal{S}_5)$ This is the bifurcation surface due to multiplicity of infinite singularities, i.e. when at least two infinite singular points coalesce. The equation of this surface is

$$\begin{aligned}\eta =& 32 - 27k^2 + 72km + 16m^2 + 32km^3 - 48n - \\ & 36kmn - 16m^2n + 24n^2 + 4m^2n^2 - 4n^3 = 0.\end{aligned}$$

The surface of C^∞ bifurcation points due to a strong saddle or a strong focus changing the sign of their traces (weak saddle or weak focus)

$(\mathcal{S}_3)$ This is the bifurcation surface due to finite singularities becoming weak, which occurs when the trace of a finite singular point is zero. The equation of this surface is given by

$$\mathcal{T}_4 = 8 - k^2 + 4n = 0,$$

where $\mathcal{T}_4$ is defined in [Vulpe, 2011].

This bifurcation can produce a topological change if the weak point is a focus or just a C^∞ change if it is a saddle, except when this bifurcation coincides with a loop bifurcation associated with the same saddle, in which case, the change may also be topological. In system (7) we shall have topological change only related to a focus becoming weak. For the other case (loop bifurcation associated with a weak saddle), see more details in [**?**].

The surface of C^∞ bifurcation due to a node becoming a focus

$(\mathcal{S}_6)$ This surface contains the points of the parameter space where a finite node of the system turns into a focus. This surface is a C^∞ but not a topological bifurcation surface. In fact, when we only cross the surface $(\mathcal{S}_6)$ in the bifurcation diagram,

the topological phase portraits do not change. However, this surface is relevant for isolating the regions where a limit cycle surrounding an antisaddle cannot exist. The equation of this surface is given by $W_4 = 0$, where

$$W_4 = 64 - 48k^2 + k^4 + 128km - 64n - 8k^2n + 16n^2.$$

6.2. Bifurcation surface due to the presence of invariant straight lines

Using the notation in [Artés *et al.*, 2008], we construct the following T–comitants:

$$\begin{aligned} B_3 &= (C_2, D)^{(1)} = \text{Jacob}\,(C_2, D)\,, \\ B_2 &= (B_3, B_3)^{(2)} - 6B_3(C_2, D)^{(3)}, \\ B_1 &= \text{Res}_x\,(C_2, D)\,/y^9 = -2^{-9}3^{-8}\,(B_2, B_3)^{(4)}\,. \end{aligned} \tag{17}$$

Lemma 6.1 ([Schlomiuk & Vulpe, 2004])**.** *For the existence of invariant straight lines under the flow of system* (7) *in one (respectively two; three distinct) directions in the affine plane it is necessary that* $B_1 = 0$ *(respectively* $B_2 = 0$*;* $B_3 = 0$*).*

Using equations (17), for system (7), we calculate:

$$\begin{aligned} B_3 =& 6mx^4 + 6(n-2)x^3y - 9kx^2y^2, \\ B_2 =& -648(4 + 2km - 4n + n^2)x^4 + \\ & 2592k(c-2)x^3y - 3888k^2x^2y, \\ B_1 =& -k^3. \end{aligned} \tag{18}$$

($\mathcal{S}_4$) This bifurcation surface is related to the existence of an invariant straight line in the phase portrait. According to Lemma 6.1, we see that $B_1 = 0$ if, and only if, $k = 0$, and this implies the existence of the invariant line $x = 0$ on the plane $k = 0$. Restricted to this plane, another invariant line is possible to exist if, and only if, $B_2 = 0$, which is equivalent to $n = 2$, and in this case, $x = 0$ is a double invariant line. Moreover, $B_3 = 0$ if, and only if, $m = 0$ and, then, the line $x = 0$ is a triple invariant line for the system.

These bifurcation surfaces are all algebraic and they, except ($\mathcal{S}_4$), are the bifurcation surfaces of singularities of systems (7) in the parameter space. We shall discover another bifurcation surface not necessarily algebraic and on which the system has global connection of separatrices. The equation of this bifurcation surface can only be determined approximately by means of numerical tools. Using arguments of continuity in the phase portraits we can prove the existence of this not necessarily algebraic component in the region where it appears, and we can check it numerically. We will name it the surface ($\mathcal{S}_7$).

We shall foliate the 3–dimensional bifurcation diagram in $\mathbb{R}^3$ by planes $k = k_0$, k_0 constant. We shall give pictures of the resulting bifurcation diagram on these planar sections on an affine chart on $\mathbb{R}^2$. With the purpose of detecting the key values for this foliation, we must find the values of parameters where the surfaces possess singularities and intersect to each other. As we mentioned before, we will be only interested in non–negative values of k to construct the bifurcation diagram.

Since the final bifurcation diagram is quite complex, it is useful to introduce colors for each one of the bifurcation surfaces, as done in previous papers of the same authors. They are:

(a) the curve obtained from the surface ($\mathcal{S}_1$) is drawn in blue (a finite singular point coalesces with an infinite one);

(b) the curve obtained from the surface ($\mathcal{S}_3$) is drawn in yellow (when the trace of a singular point becomes zero);

(c) the curve obtained from the surface ($\mathcal{S}_5$) is drawn in red (two infinite singular points coalesce);

(d) the curve obtained from the surface ($\mathcal{S}_6$) is drawn in black (an antisaddle is on the edge of turning from a node to a focus or vice versa); and

(e) the curve obtained from the surface ($\mathcal{S}_7$) is drawn in purple (the connection of separatrices).

Surface ($\mathcal{S}_4$) will be considered only for $k = 0$, and in this slice this surface corresponds to the whole plane. So, it is not necessary to assign a color to represent it.

The numeration of the surfaces is coherent with previous papers using the same technique and the

"gap $(\mathcal{S}_2)$" corresponds to a surface unnecessary here.

The following set of fourteen results study the singularities of each surface and the simultaneous intersection points of them, or the points or curves where two bifurcation surfaces are tangent.

Lemma 6.2. *Concerning the singularities of the surfaces, it follows that:*

(i) *$(\mathcal{S}_1)$ and $(\mathcal{S}_3)$ have no singularities;*

(ii) *$(\mathcal{S}_5)$ has a curve of singularities given by $6 + 4m^2 - 3n = 0$;*

(iii) *$(\mathcal{S}_6)$ has a singularity on the straight line $(m, 2, 0)$ on slice $k = 0$. Besides, this surface restricted to $k = 0$ is part of the surface $(\mathcal{S}_5)$.*

Proof. It is easy to see that the gradient of $(\mathcal{S}_1)$ and $(\mathcal{S}_3)$ is never null for all $(m, n, k) \in \mathbb{R}^3$; so *(i)* is proved. In order to prove *(ii)* we compute the gradient of η and we verify that it vanishes whenever $m = -3\sqrt[3]{k}/2$ and $n = 2 + 3\sqrt[3]{k^2}$, for all $k \geq 0$. It is easy to see that these values of m and n for all $k \geq 0$ lie on the curve $6+4m^2-3n = 0$. Finally, considering the gradient of the surface $(\mathcal{S}_6)$, it is identically zero at the point $(0, 2, 0)$ which lies on the straight line $(m, 2, 0)$ whenever $k = 0$. Moreover, if $k = 0$, we see that the equation of $(\mathcal{S}_6)$ is $(n - 2)^2$, which is part of $(\mathcal{S}_5)$, proving *(iii)*. ■

Lemma 6.3. *Surfaces $(\mathcal{S}_1)$ and $(\mathcal{S}_3)$ do not intersect on $k = 0$. For all $k \neq 0$, they intersect at the point $((k^2 - 4)/2k, -2 + k^2/4, k)$.*

Proof. By solving simultaneously both equations of the surfaces $(\mathcal{S}_1)$ and $(\mathcal{S}_3)$ for all $k \neq 0$, we obtain the point $((k^2 - 4)/2k, -2 + k^2/4, k)$. We also note that, if $k = 0$, there is no intersection point. ■

Lemma 6.4. *Surfaces $(\mathcal{S}_1)$ and $(\mathcal{S}_4)$ intersect along the curve $(m, -2, 0)$, for all $m \in \mathbb{R}$.*

Proof. It is enough to solve the system of equations of the surfaces. ■

Lemma 6.5. *Surfaces $(\mathcal{S}_1)$ and $(\mathcal{S}_5)$ intersect along the curve $\gamma_1(m, n) = 1 - 2m^2 + 2n - m^2n + n^2 = 0$, for all $k \neq 0$. Moreover, this intersection is in fact a 2–order contact.*

Proof. By solving simultaneously both equations of the surfaces $(\mathcal{S}_1)$ and $(\mathcal{S}_5)$ for $k = 0$, we do not obtain any solution. For all $k \neq 0$, the simultaneous solution of the equations is $r = ((k^2 - 4)/2k, -2 + k^2/4, k)$. If we compute the resultant with respect to k of $(\mathcal{S}_1)$ and $(\mathcal{S}_5)$, we obtain $\mathrm{Res}_k[(\mathcal{S}_1), (\mathcal{S}_5)] = 16(\gamma_1(m, n))^2\gamma_2(m, n)$, where $\gamma_1(m, n)$ is as stated in the statement of the lemma and $\gamma_2(m, n) = 64+32m^2-16n+n^2$. It is easy to see that the solution r is a double root of $(\gamma_1(m, n))^2$, proving that both surfaces intersect along $\gamma_1(m, n)$. The surfaces have a 2–order contact along the curve $\gamma_1(m, n)$. Indeed, we have just shown that the point r is a common point of both surfaces. Applying the change of coordinates given by $n = (4km - k^2 + v)/4$, $v \in \mathbb{R}$, we see that the gradient vector of $(\mathcal{S}_1)$ is $\nabla\mu(r) = (0, 1, 0)$ while the gradient vector of $(\mathcal{S}_5)$ is $\nabla\eta(r) = (0, -(k^2 + 8)^3/16k^2, 0)$, whose second coordinate is always negative for all $k \neq 0$. Since it does not change its sign, the vector $\nabla\eta(r)$ will always point towards the same direction in relation to $(\mathcal{S}_1)$ restricted to the previous change of coordinates. Then, the surface $(\mathcal{S}_5)$ remains only on one of the two topological subspaces delimited by the surface $(\mathcal{S}_1)$, proving our claim. ■

Lemma 6.6. *Surfaces $(\mathcal{S}_1)$ and $(\mathcal{S}_6)$ do not intersect on $k = 0$. For all $k \neq 0$, they have a 2–order contact along the surface $1-2m^2+2n-m^2n+n^2 = 0$.*

Proof. The proof of this lemma is analogous to the proof of Lemma 6.5. ■

Lemma 6.7. *Surfaces $(\mathcal{S}_3)$ and $(\mathcal{S}_4)$ intersect along the curve $(m, -2, 0)$, for all $m \in \mathbb{R}$.*

Proof. Analogous to Lemma 6.4. ■

Lemma 6.8. *If $k = 0$, surfaces $(\mathcal{S}_3)$ and $(\mathcal{S}_5)$ have no intersection points. For all $k \neq 0$, they intersect along the curves $\gamma_1(m, n) = 1 - 2m^2 + 2n - m^2n + n^2 = 0$ and $\gamma_3(m, n) = 256m^4 + (46 - 7n + n^2)^2 + m^2(1272 - 364n + 10n^2 - n^3) = 0$.*

Proof. Solving the system formed by the equations of the surfaces, we obtain the points: $r_1 = ((k^2 - 4)/2k, -2 + k^2/4, k)$, $r_2 = (-(32k + k^3 + \sqrt{(k^2 - 64)^3})/256, -2+k^2/4, k)$ and $r_3 = (-(32k+k^3 - \sqrt{(k^2 - 64)^3})/256, -2 + k^2/4, k)$. It is easy to

verify that r_1 is the only solution of $\gamma_1(m,n)=0$ and r_2 and r_3 are the solutions of $\gamma_3(m,n)=0$. ■

Corollary 6.9. *If $k=8$, the points r_2 and r_3 of Lemma 6.8 are equal and they correspond to the singularity of the surface $(\mathcal{S}_5)$.*

Proof. Replacing $k=8$ in the expressions of the points r_1, r_2 and r_3 described in Lemma 6.8, we see that $r_2=r_3$ and they are equal to the singularity $(-3,14,8)$ of the surface $(\mathcal{S}_5)$. ■

Lemma 6.10. *If $k=0$, surfaces $(\mathcal{S}_3)$ and $(\mathcal{S}_6)$ have no intersection points. For all $k\neq 0$, they intersect along the curve $\gamma(m,n)=1-2m^2+2n-m^2n+n^2=0$.*

Proof. The proof follows straightforwardly from the common solution of the system formed by the equations of both surfaces. ■

Lemma 6.11. *Surfaces $(\mathcal{S}_4)$ and $(\mathcal{S}_5)$ intersect along the curves $(m,-2,0)$ and $(m,2+m^2,0)$, for all $m\in\mathbb{R}$.*

Proof. Analogous to Lemma 6.4. ■

Lemma 6.12. *Surfaces $(\mathcal{S}_4)$ and $(\mathcal{S}_6)$ intersect along the curve $(m,-2,0)$, for all $m\in\mathbb{R}$.*

Proof. Analogous to Lemma 6.4. ■

Lemma 6.13. *If $k=0$, surfaces $(\mathcal{S}_5)$ and $(\mathcal{S}_6)$ intersect along the straight line $(m,2,0)$, for all $m\in\mathbb{R}$. For all $k\neq 0$, they have a 2–order contact point at $r_1=((k^2-4)/2k,-2+k^2/4,k)$ and intersection points at*

$$\begin{aligned} r_{2,3}=\big(&-(64-48k^2+k^4-4\alpha/3-k^2\alpha/6+\\ &\alpha^2/144)/128k,(48+5k^2)/24-(1\pm i\sqrt{3})\times\\ &(-442368k^2-256k^4)/(12288\gamma)+\\ &(1\mp i\sqrt{3})\gamma/48,k\big),\end{aligned}$$

$$\begin{aligned} r_4=\big(&(-k^8-16\sqrt{6k^4(216-k^2)^3}\beta-k^6(\beta-1728)-\\ &k^4(746496-288\beta+\beta^2)-32k^2(\sqrt{6k^4(216-k^2)^3}-\\ &3888\beta+12\beta^2))/(1536k\beta^2),(48+5k^2)/24-\\ &(442368k^2+256k^4)/(6144\gamma)-\gamma/24,k\big),\end{aligned}$$

where

$$\begin{aligned} \alpha=&96+10k^2+(1\pm i\sqrt{3})k^2(1728+k^2)/\beta+(1\mp i\sqrt{3})\beta,\\ \beta=&\big(k^6-4320k^4-373248k^2+48\sqrt{6k^4(216-k^2)^3}\big)^{1/3},\\ \gamma=&\big(k^6-373248k^2-4320k^4+48\sqrt{6}\times\\ &\sqrt{10077696k^4-139968k^6+648k^8-k^{10}}\big)^{1/3}.\end{aligned}$$

Proof. Replacing $k=0$ in the equations of the surfaces and solving them in the variables m and n, we find that $m\in\mathbb{R}$ and $n=2$, implying the existence of intersection along the straight line $(m,2,0)$, $m\in\mathbb{R}$. For all $k\neq 0$, we solve the equation of surface $(\mathcal{S}_5)$ with respect to m and substitute it in the equation of surface $(\mathcal{S}_6)$, obtaining $W_4\big|_{\eta=0}=(k^2-4n-8)^2(128k^4-k^6+1536n-832k^2n+16k^4n-768n^2-80k^2n^2+128n^3-4928k^2-1024)/65536$. Then, we see that the intersection of these two surfaces has two branches. On one of these branches, namely $k^2-4n-8=0$, we obtain the point $r_1=((k^2-4)/2k,-2+k^2/4,k)$. Since this factor is double, we conclude that r_1 is a 2–order contact point of both surfaces. On the other branch, we obtain the intersection points r_2, r_3 and r_4 described in the statement of the lemma, and we finish the proof. ■

Remark 6.14. The notation $r_{2,3}$ in the statement of Lemma 6.13 means that we need to consider the different signs in r_2 with relation to r_3, i.e.

$$\begin{aligned} r_2=\big(&-(64-48k^2+k^4-4\alpha/3-k^2\alpha/6+\\ &\alpha^2/144)/128k,(48+5k^2)/24-(1+i\sqrt{3})\times\\ &(-442368k^2-256k^4)/(12288\gamma)+\\ &(1-i\sqrt{3})\gamma/48,k\big),\end{aligned}$$

with

$$\alpha=96+10k^2+(1+i\sqrt{3})k^2(1728+k^2)/\beta+(1-i\sqrt{3})\beta,$$

and β and γ as in the statement, and

$$\begin{aligned} r_3=\big(&-(64-48k^2+k^4-4\alpha/3-k^2\alpha/6+\\ &\alpha^2/144)/128k,(48+5k^2)/24-(1-i\sqrt{3})\times\\ &(-442368k^2-256k^4)/(12288\gamma)+\\ &(1+i\sqrt{3})\gamma/48,k\big),\end{aligned}$$

with

$$\alpha=96+10k^2+(1-i\sqrt{3})k^2(1728+k^2)/\beta+(1+i\sqrt{3})\beta,$$

and β and γ as in the statement.

Remark 6.15. Recalling the intersection points of surfaces $(\mathcal{S}_5)$ and $(\mathcal{S}_6)$ obtained in Lemma 6.13, we observe that points r_1 and r_2 are real for all $k \geq 0$. In contrast, points r_3 and r_4 are real only for $k \geq 6\sqrt{6}$, since

$$\begin{aligned}\text{Discrim}_n \big[128k^4 - k^6 + 1536n - 832k^2n + 16k^4n - \\ 768n^2 - 80k^2n^2 + 128n^3 - 4928k^2 - \\ 1024\big] = 2097152k^4(k^2 - 216)^3,\end{aligned}$$

and substituting the value of k in the expression inside the discriminant by any value less than $6\sqrt{6}$, we obtain a real solution (namely, r_2) and two conjugate complex solutions (namely, r_3 and r_4). And when $k = 6\sqrt{6}$, we have $r_3 \equiv r_4$.

The purpose now is to find the slices on which there exists intersection of two or more surfaces or other equivalent phenomena happen. Since there exist 12 distinct curves of intersection or contact of two any surfaces, we need to study 66 different possible intersections of these surfaces. Even though this relation is long, only five of them provide substantial information for our study. The remaining cases reveal that some curves are identical or they do not intersect. We will reproduce here only these five relations. The full set of proves can be found on the web page http://mat.uab.es/∼artes/articles/qvfts/qvfts.html.

Remark 6.16. In the next two lemmas we use the following notation. A curve of intersection or contact between two surfaces will be denoted by *solAByC*, where $A < B$ are the numbers of the surfaces involved in the intersection or contact and C is a cardinal.

Lemma 6.17. *The singularity of surface* $(\mathcal{S}_5)$ *intersects surface* $(\mathcal{S}_3)$ *for* $k = 8$.

Proof. By Lemmas 6.2 and 6.8, we have the curves sol35y2 $= (-(32k + k^3 + \sqrt{(k^2-64)^3})/256, -2 + k^2/4, k)$, sol35y3 $= (-(32k + k^3 - \sqrt{(k^2-64)^3})/256, -2 + k^2/4, k)$ and sol55y1 $= (-3\sqrt[3]{k}/2, 2 + 3\sqrt[3]{k^2}, k)$. By equalizing each corresponding coordinates of the pairs sol35y2, sol35y3, sol35y2, sol55y1 and sol35y3, sol55y1, and solving the obtained systems, we have the solution $k = 8$. ∎

Lemma 6.18. *The singularity of surface* $(\mathcal{S}_5)$ *intersects surface* $(\mathcal{S}_6)$ *for* $k = 6\sqrt{6}$.

Proof. By Lemmas 6.2 and 6.13, we have the curves sol55y1 $= (-3\sqrt[3]{k}/2, 2 + 3\sqrt[3]{k^2}, k)$ sol56y3 $= r_3$ and sol56y4 $= r_4$ (*cf.* Lemma 6.13). By equalizing each corresponding coordinates of the pairs sol55y1, sol56y4 and sol56y3, sol56y4, and solving the obtained systems, we have the solution $k = 6\sqrt{6}$. ∎

Remark 6.19. Lemma 6.17 describes the behavior of the curves of intersections of surfaces $(\mathcal{S}_3)$ and $(\mathcal{S}_5)$ with the singularity of surface $(\mathcal{S}_5)$. That is to say that, when $k = 8$, the singularity of surface $(\mathcal{S}_5)$ coincides with the two intersection points of surfaces $(\mathcal{S}_3)$ and $(\mathcal{S}_5)$ (for an illustration of this fact, see Figs. 7 to 9). Lemma 6.18 indicates when the singularity of surface $(\mathcal{S}_5)$ lies on surface $(\mathcal{S}_6)$, implying that two of the points of intersection of surfaces $(\mathcal{S}_5)$ and $(\mathcal{S}_6)$ coincide with this singularity (for an illustration of this fact, see Figs. 9 to 11).

The next result presents all the algebraic values of k corresponding to singular slices in the bifurcation diagram. Its proof follows from Lemmas 6.3 to 6.18.

Lemma 6.20. *The full set of needed algebraic singular slices in the bifurcation diagram of family* $\mathbf{QT\overline{S}}$ *is formed by* 3 *elements which correspond to the values*

$$k_1 = 6\sqrt{6}, \quad k_3 = 8, \quad k_9 = 0. \tag{19}$$

The numeration in (19) is not consecutive since we reserve numbers for other slices not algebraically determined and for generic slices.

Now we sum up the content of the previous lemmas. In (19) we list all the algebraic values of k where significant phenomena occur for the bifurcation diagram generated by singularities. We first have the two extreme values for k, i.e. $k = 0$ and $k = 6\sqrt{6}$.

In order to determine all the parts generated by the bifurcation surfaces from $(\mathcal{S}_1)$ to $(\mathcal{S}_7)$, we first draw the horizontal slices of the three–dimensional parameter space which correspond to the explicit values of k obtained in Lemma 6.20. However, as it will be discussed later, the presence of nonalgebraic

bifurcation surfaces will be detected and the singular slices corresponding to their singular behavior as we move from slice to slice will be approximately determined. We add to each interval of singular values of k an intermediate value for which we represent the bifurcation diagram of singularities. The diagram will remain essentially unchanged in these open intervals except the parts affected by the bifurcation. All the sufficient values of k are shown in (20):

$$\begin{gathered} k_0 = 16,\ k_1 = 6\sqrt{6},\ k_2 = 9, \\ k_3 = 8,\ k_4 = 8 - \varepsilon_1,\ k_5 = 8 - \varepsilon_2^*, \\ k_6 = 8 - \varepsilon_3,\ k_7 = 8 - \varepsilon_4^*,\ k_8 = 4,\ k_9 = 0. \end{gathered} \tag{20}$$

The values indexed by odd indices in (20) correspond to the values of k for which there exists a bifurcation in the behavior of the systems on the slices. Those indexed by even values are just intermediate points which are necessary for the coherence of the bifurcation diagram.

Due to the presence of some branches of non-algebraic bifurcation surfaces, we cannot point out exactly the concrete value of k where the changes in the parameter space happen. Thus, with the purpose to set an order for these changes, we introduce the following notation. If the bifurcation happens between two concrete values of k, then we add or subtract a sufficiently small positive value ε_i or ε_j^* to/from a concrete value of k; this concrete value of k (which is a reference value) can be any of the two values that define the range where the non–concrete values of k are inserted. The representation ε_i means that the k_i refers to a generic slice, whereas ε_j^* means that the k_j refers to a singular slice. Moreover, considering the values ε_i, ε_i^*, ε_{i+1} and ε_{i+1}^*, it means that $\varepsilon_i < \varepsilon_i^* < \varepsilon_{i+1} < \varepsilon_{i+1}^*$ meanwhile they belong to the same interval determined by algebraic bifurcations.

We now begin the analysis of the bifurcation diagram by studying completely one generic slice and then moving from slice to slice and explaining all the changes that occur. As an exact drawing of the curves produced by intersecting the surfaces with the slices gives us very small parts which are difficult to distinguish, and points of tangency are almost impossible to recognize, we have produced topologically equivalent figures where parts are enlarged and tangencies are easy to observe.

The reader may find the exact pictures as well as most of the proves of this study in the web page http://mat.uab.es/∼artes/articles/qvfts/qvfts.html.

Notation. The description of the labels used for each part of the bifurcation space is as follows. The subsets of dimensions 3, 2, 1 and 0, of the partition of the parameter space will be denoted respectively by V, S, L and P for Volume, Surface, Line and Point, respectively. The surfaces are named using a number which corresponds to each bifurcation surface which is placed on the left side of the letter S. To describe the portion of the surface we place an index. The curves that are intersection of surfaces are named by using their corresponding numbers on the left side of the letter L, separated by a point. To describe the segment of the curve we place an index. Volume and Point are simply indexed (since three or more surfaces may be involved in such an intersection).

We consider an example: surface $(\mathcal{S}_1)$ splits into 2 different two–dimensional parts labeled as $1S_1$ and $1S_2$, plus some one–dimensional arcs labeled as $1.iL_j$ (where i denotes the other surface intersected by $(\mathcal{S}_1)$ and j is a number), and some zero–dimensional parts. In order to simplify the labels in all figures we see **V1** which stands for the TEX notation V_1. Analogously, **1S1** (respectively, **1.3L1**) stands for $1S_1$ (respectively, $1.3L_1$). And the same happens with many other pictures.

In Fig. 2 we represent the generic slice of the parameter space when $k = k_0 = 16$, showing only the algebraic surfaces. We note that there is a dashed branch of surface $(\mathcal{S}_3)$ (in yellow). This means the existence of a weak saddle and it does not produce a topological change in the phase portraits but a C^∞ change. In the next figures we will use the same representation for this characteristic of this surface. Instead, even if surface $(\mathcal{S}_6)$ (in black) does not produce any topological change in the phase portraits, we draw it continuously.

Remark 6.21. Wherever two parts of equal dimension d are separated only by a part of dimension $d-1$ of the black bifurcation surface $(\mathcal{S}_6)$, their respective phase portraits are topologically equivalent since the only difference between them is that a finite antisaddle has turned into a focus without change of stability and without appearance of limit cycles. We denote such parts with different labels, but we do not give specific phase portraits in pic-

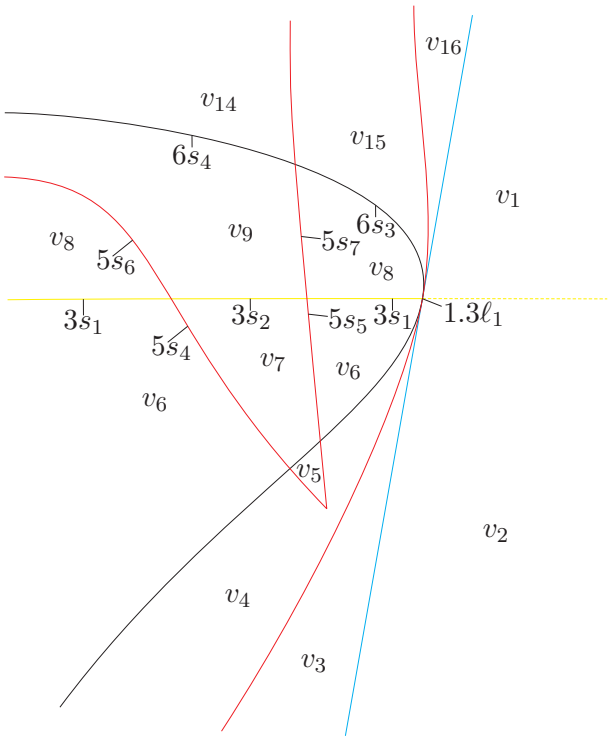

Fig. 2. Slice of parameter space when $k = 16$ (only algebraic surfaces)

tures attached to Theorem 1.1 for the parts with the focus. We only give portraits for the parts with nodes, except in the case of existence of a limit cycle or a graphic where the singular point inside them is portrayed as a focus. Neither do we give specific invariant description in Sec. 8 distinguishing between these nodes and foci.

6.3. Bifurcation surfaces due to connections of separatrices

We start this section explaining the generic slice when $k = 16$. In this slice we will make a complete study of all its parts, whereas in the next slices we will only describe the few changes which occur.

As said in last section, in Fig. 2 we present the slice when $k = 16$ with only the algebraic surfaces. For each set of the partition on this slice, we consider a specific value of the parameters of the system and compute the global phase portrait with the numerical program P4 [Dumortier *et al.*, 2006]. In fact, all the phase portraits in this study can be obtained not only numerically but also by means of perturbations of the systems of codimension three.

In this slice we have a partition in 2−dimensional parts bordered by curved polygons, some of them bounded, others bordered by infinity. From now on, we use lower–case letters provisionally to describe the sets found algebraically with the purpose of not interfering with the final partition described with capital letters.

For each 2−dimensional part of Fig. 2 we obtain a phase portrait which is coherent with those of all their borders. Except for two parts:

- v_8: having two connected components, one of them being the curved triangle bordered by yellow, red and black curves and the other being bordered by yellow and red curves and infinity;

- v_9: the curved polygon bordered by yellow, black and two branches of red curves and infinity.

Remark 6.22. We observe that we have named pairs of regions in Fig. 2 with the same label because they are in fact the same part, i.e. although they appear in the affine charts of $\mathbb{R}^2$ with two connected components, they are in fact the same parts if we visualize them in $\mathbb{R}^3$. It will become clearer as we describe the transition from slice to slice.

We consider the connected component of part v_6 which has $5s_4$ as a border. The phase portrait of this part is shown in Fig. 3 with a repeller focus. When we go towards part v_8 crossing $3s_1$, the focus becomes attractor, i.e. on $3s_1$ the repeller focus becomes weak, a Hopf bifurcation happens when we enter in part v_8 and a limit cycle is born. Analogously, we have the same phenomenon happening in the bounded components of parts v_6, $3s_1$ and v_8.

Following the same steps, we verify that in part v_9 we must also have a limit cycle around the focus which was generated by a Hopf bifurcation after crossing $3s_2$ from v_7. See Fig. 3 for an illustration of the transitions just described.

However, if we move in the contrary direction, we are able to find values for the parameters in parts v_8 and v_9 for which the phase portraits have no limit cycles.

More specifically, if we start from part v_{15}, whose phase portrait is shown in Fig. 4, and move towards part v_8, the attracting node turns into an

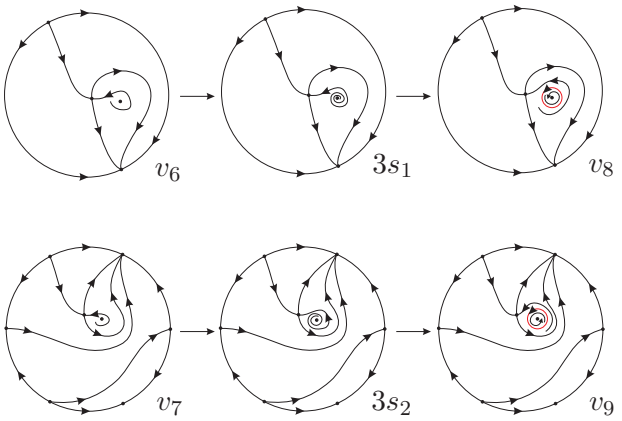

Fig. 3. Transitions from parts v_6 to v_8 and from v_7 to v_9 passing through $3s_1$ and $3s_2$, respectively. A limit cycle is born by a Hopf bifurcation in v_8 (respectively, v_9) after crossing $3s_1$ (respectively, $3s_2$) from v_6 (respectively, v_7)

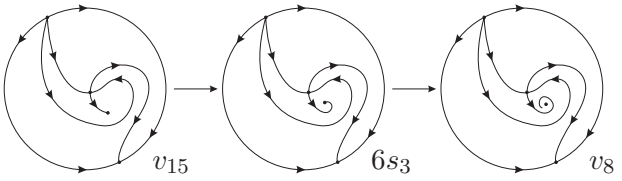

Fig. 4. Transitions from parts v_{15} to v_8 crossing $6s_3$

attracting focus (causing only a C^∞ change in the phase portrait) due to the bifurcation of surface ($\mathcal{S}_6$) on segment $6s_3$. In this sense, we have two topologically distinct phase portraits in part v_8 (one of them with limit cycle and the other one without it). So, it suggests the existence of at least one branch of a new surface ($\mathcal{S}_7$) which divides region v_8.

Analogously, moving from v_{14} to v_9, passing through $6s_4$, we find a topologically distinct phase portrait for part v_9 ($v_9(c)$ in Fig. 5) in comparison to the one obtained before. This fact also implies the existence of at least one branch of surface ($\mathcal{S}_7$) which divides region v_9.

We claim that there must exist at least two branches of surface ($\mathcal{S}_7$) dividing parts v_8 and v_9. Indeed, we start from part v_9. According to what was discussed above, the phase portrait of region v_9 in the neighborhood of segment $3s_2$ possesses a limit cycle around the attractor focus. In order to loose it when we move towards part v_{14}, a bifurcation must occur. The most likely to happen is a bifurcation of separatrix connection due to that fact that there

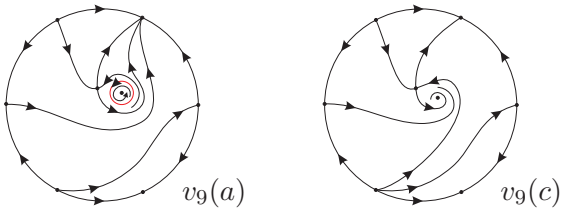

Fig. 5. Two phase portraits of part v_9 found until now. Portrait $v_9(a)$, in the neighborhood of segment $3s_2$, possesses limit cycle, whereas in $v_9(c)$, in the neighborhood of segment $6s_4$, the limit cycle has already disappeared. It suggests the existence of at least one more partition of v_9

exist no other branches of surface ($\mathcal{S}_3$) (in yellow) rather than $3s_2$ which borders part v_9 (i.e. it is not possible to occur another Hopf bifurcation inside v_9).

Analyzing Fig. 5, we see that both phase portraits $v_9(a)$ and $v_9(c)$ are not coherent, not even if we consider a single portrait representing a connection of separatrices. It is necessary another partition of v_9 for which the transition from phase portrait $v_9(a)$ to $v_9(c)$ becomes totally coherent. Two separatrices of the finite saddle must connect into a loop, which makes the limit cycle disappears. Then, part v_9 must be split into three distinct regions V_9, V_{11} and V_{13} (modulo islands; see Sec.7) by two segments of surface ($\mathcal{S}_7$) named $7S_2$ and $7S_4$ referring to a loop connection and a finite–infinite saddle connection, respectively. Fig. 6 illustrates the transition of the phase portraits moving from v_7 to v_{14}, passing through v_9.

It is worth mentioning that the bifurcations just described must occur in the order set above (considering that we are moving from v_7 to v_{14}), i.e. firstly the limit cycle must disappear by the loop bifurcation and then the separatrices of the finite and infinite saddles must connect, even if this order could be reversed. Indeed, if the loop bifurcation had not happened, it would be impossible to connect a separatrix of the finite saddle with the separatrix of the infinite saddle to obtain a phase portrait topologically equivalent to the one in v_{14}.

This phenomenon can also be verified by "walking" along part $5s_6$ and $5s_7$ and checking that each one of these parts presents five topologically distinct phase portraits: $5S_6$, $5.7L_1$, $5S_8$, $5.7L_3$ and $5S_{10}$ on part $5s_6$, and $5S_7$, $5.7L_2$, $5S_9$, $5.7L_4$ and

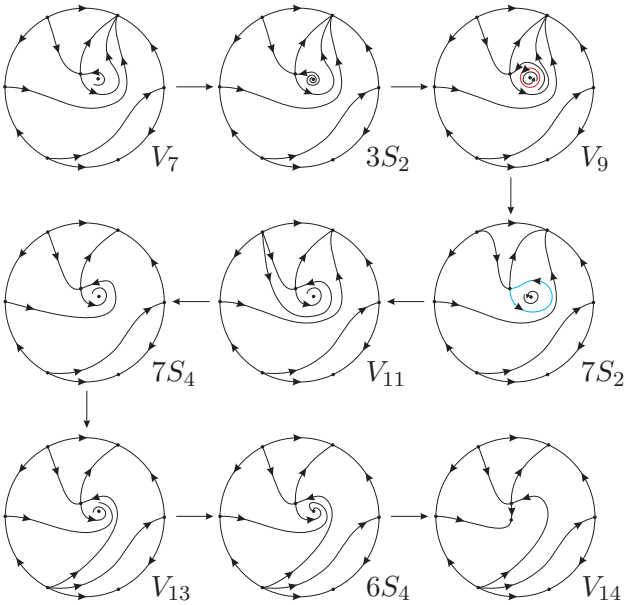

Fig. 6. Transition of the phase portraits moving from v_7 to v_{14}, passing through v_9. We start in part v_7, whose phase portrait is V_7. Then, on $3s_2$ the repeller node becomes weak (portrait $3S_2$) and a limit cycle is born when we enter part v_9 (see phase portrait V_9). In what follows, two separatrices of the finite saddle connect into a loop causing the death of the limit cycle, which leads to phase portrait $7S_2$. After the break of this loop, we obtain phase portrait V_{11} and portrait $7S_4$ shows the connection of the separatrices of the finite saddle and the infinite saddle. In this way, we have phase portrait V_{13} and when we lie on $6s_4$ the focus is in turn to become a node (see portrait $6S_4$) and, finally, we have the phase portrait V_{14} of part v_{14}

$5S_{11}$ on part $5s_7$. See Fig. 7 for a complete picture of the bifurcation diagram for slice $k = 16$.

Analogously, we have the same behavior in part v_8, but with a subtle difference. The branch of surface ($\mathcal{S}_7$) referring to the loop connection is the continuation of segment $7S_2$ and it is named $7S_1$, possessing two connected components (one of them being bounded and the other unbounded). In v_8, the finite–infinite connection does not cause any topological change in the phase portraits (only a C^∞ change) because all the phase portraits of this part possess a single infinite singularity (a node) without separatrices. So, the finite–infinite saddle connection of separatrices is non–sense here. In this way, the continuation $7S_3$ of segment $7S_4$ is drawn in dashes in Fig. 7.

The regions painted in light yellow in Fig. 7

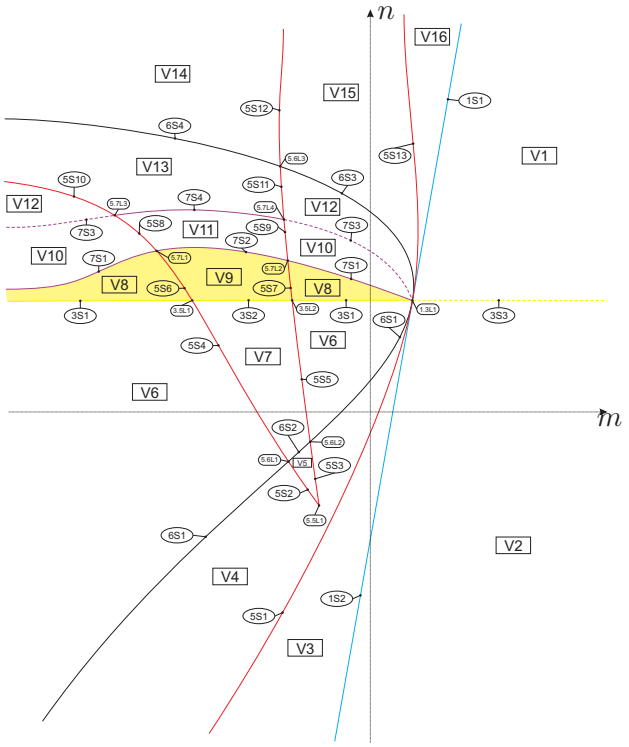

Fig. 7. Slice of parameter space when $k = 16$ (with non–algebraic algebraic surfaces)

represent regions with limit cycle.

The next result assures us the location and the position of segment $7S_1$.

Lemma 6.23. *The bounded connected component of $7S_1$ starts (or ends) at $1.3\ell_1$ and joins with segment $7S_2$ at $5.7L_2$. The unbounded connected component of $7S_1$ starts (or ends) at $5.7L_1$, which is the intersection of $7S_2$, $5S_6$ and $5S_8$.*

Proof. Numerical analysis suggests that the curve $7S_1$, which corresponds to a loop bifurcation, has one of its ends at the point $1.3\ell_1$. Indeed, if the starting point of $7S_1$ were any point of segments $3s_1$ or $6s_3$, we would have the following incoherences. Firstly, if this starting point were on $3s_1$, then a portion of this subset must not refer to a Hopf bifurcation, which contradicts the fact that on $3s_1$ we have a weak focus of order one and, since its second Lyapunov coefficient $\mathcal{F}_1 = -3k$ is constant for all $k \geq 0$ (*cf.* [Vulpe, 2011], page 6556), the trace of this focus does not change its sign. Secondly, if the starting point were on $6s_3$, then a portion of part v_{15} must lead to phase portraits with limit cycle since

surface ($\mathcal{S}_6$) (in black) refers to a C^∞ bifurcation (focus becoming a node); however, we would have a limit cycle with a node inside, which contradicts item (iii) of Sec. 4.

Since we find the existence of a loop bifurcation on $5s_6$ and $5s_7$, then, by continuity of the bifurcation diagram, $7S_1$ must be linked with $7S_2$ on these segments.

The unbounded connected component of $7S_1$, which is linked with $7S_2$ on $5s_6$, does not cross segment $3s_1$ as explained above and it does not cross segment $5s_6$ because, after some numerical experiments, we found that if we walk on the straight line $n = 68$ and consider negative values of m, the limit cycle disappears after the creation of a loop. So, it tends to infinity asymptotically to $3s_1$. ■

Since segment $7S_4$ refers to a finite–infinite saddle connection bifurcation, it only makes sense in part v_9, because the phase portraits of part v_8 does not have the infinite saddle (it becomes a complex singular point when we cross segments of surface ($\mathcal{S}_5$) (in red)). So, the only important parts of surface ($\mathcal{S}_7$) related to the finite–infinite saddle separatrix connection that provide a topological change in phase portraits are $7S_4$ and its intersections $5.7L_3$ and $5.7L_4$ with surface ($\mathcal{S}_5$). The segments which compose $7S_3$ lead to a C^∞ change in the phase portraits and then they are drawn with dashes in Fig. 7.

After this analysis, there are no other relevant non–algebraic surfaces to be consider in order to keep the coherence of the bifurcation diagram in slice $k = 16$ shown in Fig. 7. However, we cannot be sure that these are all the additional bifurcation curves in this slice because there could exist others which escaped our numerical research.

For all other two–dimensional parts of the partition of this slice, whenever we join two points which are close to different borders of the part, the two phase portraits are topologically equivalent. So, we do not encounter more situations than the ones mentioned above. In short, it is expected that the complete bifurcation diagram for $k = 16$ is the one shown in Fig. 7. More considerations about other branches of bifurcation surfaces possible to exist are considered in Sec. 7.

In what follows, we decrease the values of k, according to the values in (20), and make an analogous study for each one of the slices that we need

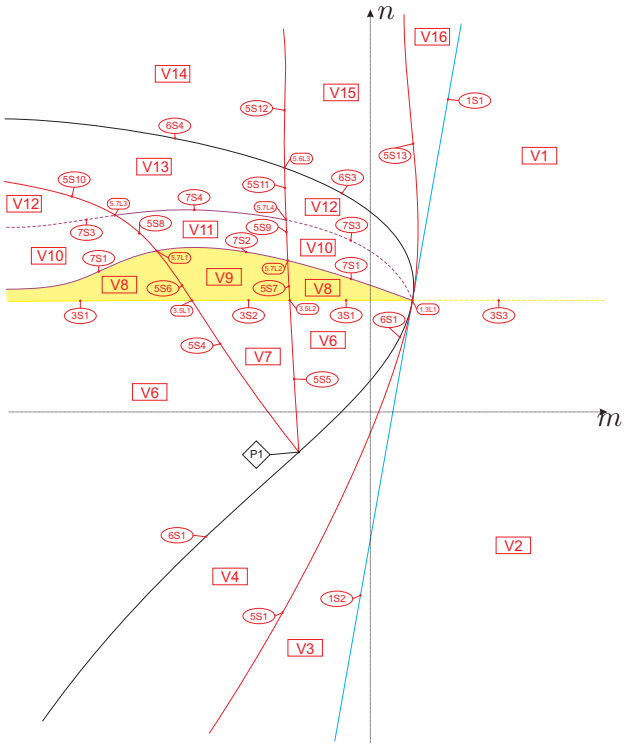

Fig. 8. Slice of parameter space when $k = 6\sqrt{6}$

to consider and also look for changes when going from one slice to the next one. Essentially, when we consider decreasing values of k in the interval $(0, +\infty)$, the coordinate n of the singularity of the red curve (hereinafter called red cusp) increases and the red cusp crosses some other curves as we shall see in the next steps. From now on, the pictures of the slices present all the algebraic and the nonalgebraic curves, since these last ones are decisive for the number of slices, according to (20).

We consider the singular slice when $k = k_1 = 6\sqrt{6}$. According to Lemma 6.18, the red cusp is on the black curve, as we can see in Fig. 8. We point out that the labels colored in red in Fig. 8 (and in the next pictures of slices) refer to regions which persist from previous slices.

When $k = k_2 = 9$, the red cusp leaves the black curve leading to region $5.5L_2$, as shown in Fig 9. Table 1 presents the dead and the born parts in the transition from the generic slice $k = 16$ to the next generic slice $k = 9$ passing through the singular slice $k = 6\sqrt{6}$.

Then, according to Lemma 6.17, the red cusp lies on the yellow curve for $k = k_3 = 8$, as shown in Fig 10. Now, according to Lemma 6.20, the next (al-

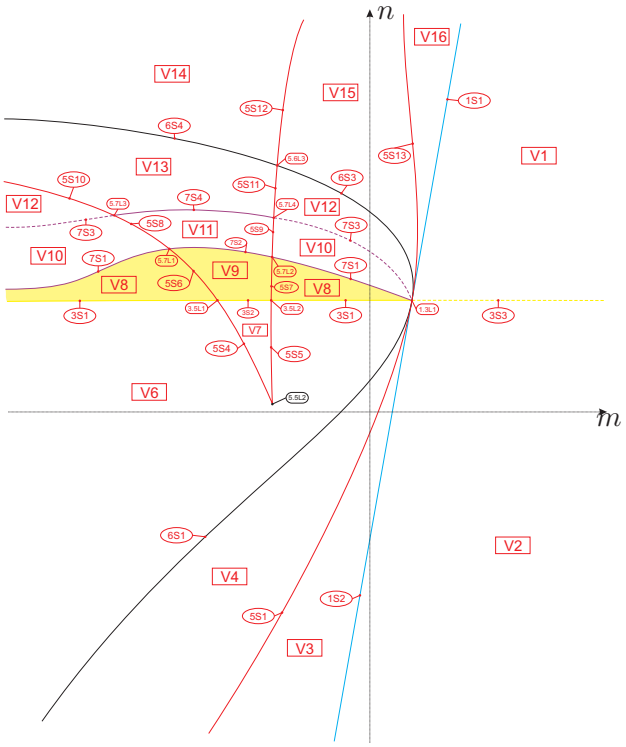

Fig. 9. Slice of parameter space when $k = 9$

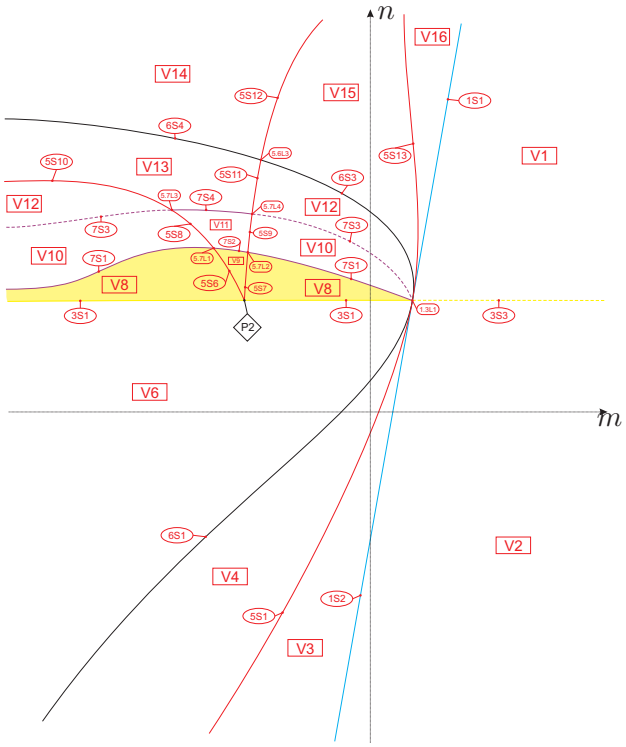

Fig. 10. Slice of parameter space when $k = 8$

Table 1. Transition from slice $k = 16$ to $k = 9$

Dead parts	Parts in Sing. Slice	Born parts
V_5, $5S_2$, $5S_3$ $6S_2$, $5.5L_1$ $5.6L_1$, $5.6L_2$	P_1	$5.5L_2$

gebraic) singular slice is for $k = 0$. However, there must exist at least two more singular values of k in the interval $(0, 8)$ due to the existence of the two branches of surface $(\mathcal{S}_7)$ already explained. Indeed, choosing different values for $k \in (0, 8)$, we observe that the movement of the separatrices of the finite saddle and the obtained phase portraits for the red cusp are coherent with the existence of these two branches of surface $(\mathcal{S}_7)$.

We consider the value $k = k_4 = 8 - \varepsilon_1$, where $\varepsilon_1 > 0$ is sufficiently small to make the red cusp lying on the region with limit cycle, as it can be seen in Fig 11, and we have the phase portrait $5.5L_3$ possessing a limit cycle. Table 2 presents the dead and the born parts in the transition from the generic slice $k = 9$ to the next generic slice $k = 8 - \varepsilon_1$ passing through the singular slice $k = 8$.

Table 2. Transition from slice $k = 9$ to $k = 8 - \varepsilon_1$

Dead parts	Parts in Sing. Slice	Born parts
V_7, $3S_2$, $5S_4$ $5S_5$, $3.5L_1$ $3.5L_2$, $5.5L_2$	P_2	$5.5L_3$

Now, we choose $\varepsilon_2^* > 0$ so that the red cusp lies on the purple curve creating the region P_3 and being bordered by the two connected segments of $7S_1$. Fig 12 illustrates the bifurcation diagram for the singular slice $k = k_5 = 8 - \varepsilon_2^* (\approx 6.1569...)$.

Next, we take $\varepsilon_3 > 0$ such that, for $k = k_6 = 8 - \varepsilon_3$, the red cusp belongs to a region surrounded by V_{10} (see Fig. 13). Table 3 presents the dead and the born parts in the transition from the generic slice $k = 8 - \varepsilon_1$ to the next generic slice $k = 8 - \varepsilon_3$ passing through the singular slice $k = 8 - \varepsilon_2^*$.

Let $\varepsilon_4^* > 0$ such that the red cusp lies on the purple curve creating the region P_4 and being bordered by the two connected segments of $7S_3$. This phenomenon occurs in slice $k = k_7 = 8 - \varepsilon_4^* (\approx$

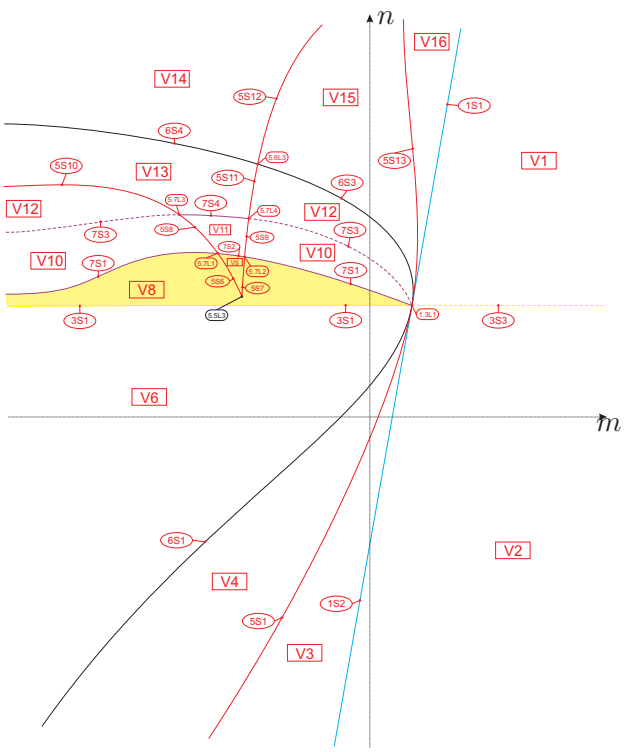

Fig. 11. Slice of parameter space when $k = 8 - \varepsilon_1$

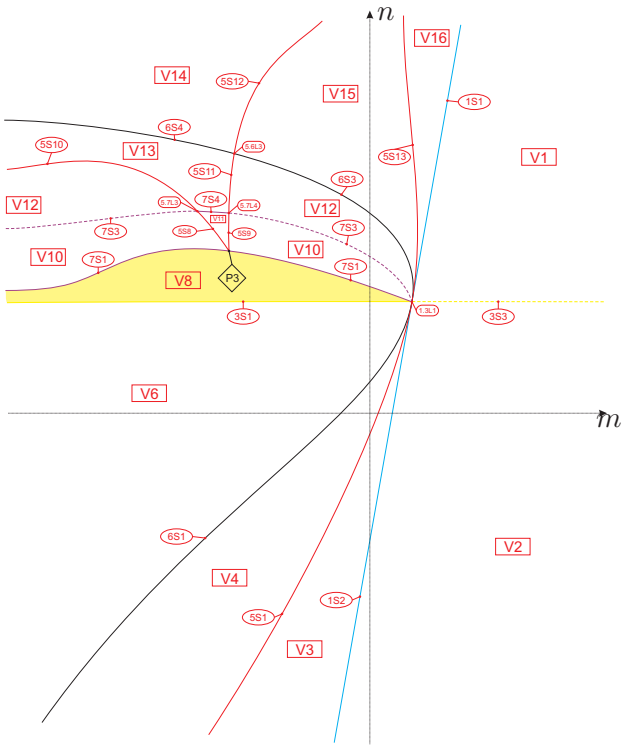

Fig. 12. Slice of parameter space when $k = 8 - \varepsilon_2^*(\approx 6.1569...)$

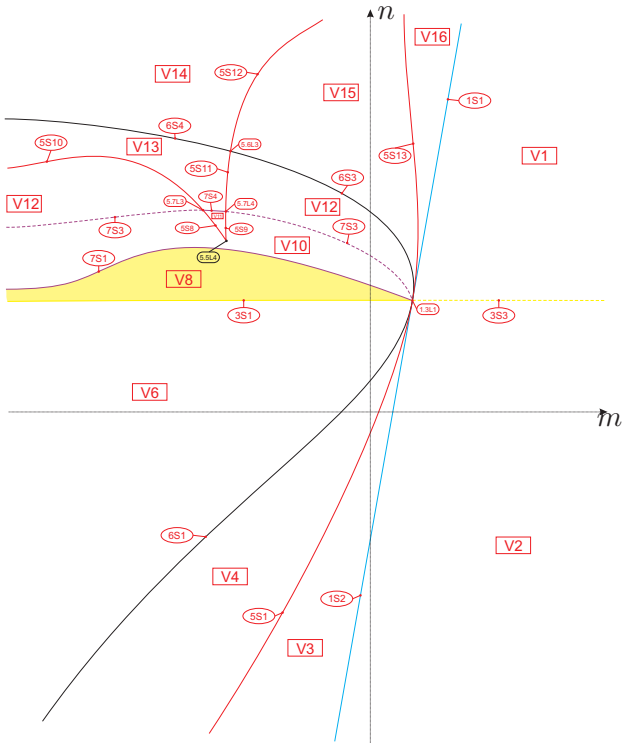

Fig. 13. Slice of parameter space when $k = 8 - \varepsilon_3$

Table 3. Transition from slice $k = 8 - \varepsilon_1$ to $k = 8 - \varepsilon_3$

Dead parts	Parts in Sing. Slice	Born parts
V_9, $5S_6$, $5S_7$ $7S_2$, $5.5L_3$ $5.7L_1$, $5.7L_2$	P_3	$5.5L_4$

5.3687...) and the bifurcation diagram for this slice is illustrated in Fig. 14.

For any $k \in (0, 8 - \varepsilon_4^*)$, the red cusp does not intersect any other curve in consideration. The bifurcation diagram for any $k \in (0, 8 - \varepsilon_4^*)$ is topologically equivalent to the one represented in Fig. 15 for $k = k_8 = 4$. Table 4 presents the dead and the born parts in the transition from the generic slice $k = 8 - \varepsilon_3$ to the next generic slice $k = 4$ passing through the singular slice $k = 8 - \varepsilon_4^*$.

It is worth noting that, although the phase portraits $5.5L_4$, $5.5L_5$ and P_4 are topologically equivalent (as we shall see it in Table 8, line 3), they have a qualitative difference. They are characterized by having a semi–elemental triple node at infinity, $\overline{\binom{0}{3}}N$. Geometrically, this infinite singular point is

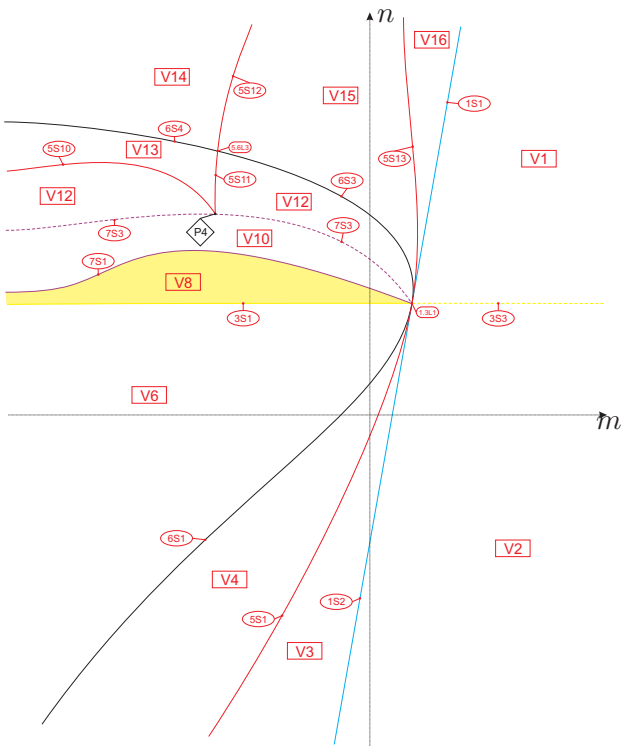

Fig. 14. Slice of parameter space when $k = 8 - \varepsilon_4^* (\approx 5.3687...)$

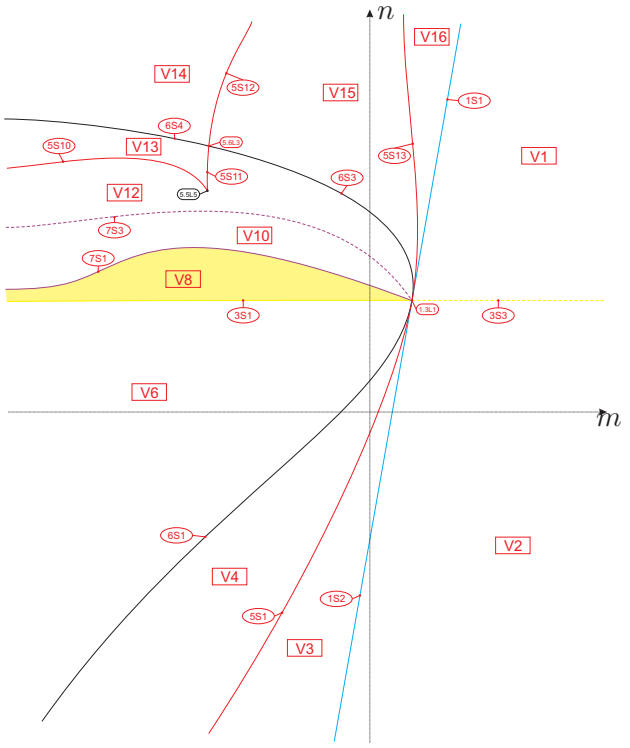

Fig. 15. Slice of parameter space when $k = 4$

Table 4. Transition from slice $k = 8 - \varepsilon_3$ to $k = 4$

Dead parts	Parts in Sing. Slice	Born parts
V_{11}, $5S_8$, $5S_9$ $7S_4$, $5.5L_4$ $5.7L_3$, $5.7L_4$	P_4	$5.5L_5$

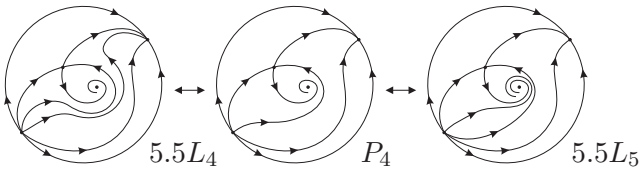

Fig. 16. Transition of the integral lines in the phase portraits $5.5L_4$, P_4 and $5.5L_5$. Even though these phase portraits are all topologically equivalent, they possess a qualitative difference: the position of the separatrix of the infinity saddle, which is joint in $\overline{\binom{0}{3}}N$, with relation to one of the separatrices of the finite saddle. This qualitative difference marks the bifurcation associated to the segments $7S_3$ and $7S_4$

formed by the coalescence of two infinite nodes and one infinite saddle. All the orbits arriving to (or departing from) this point do it tangentially to infinity except for one orbit which does it transversally. This orbit becomes the separatrix of the saddle when a perturbation splits $\overline{\binom{0}{3}}N$ in three singular points. Phase portrait P_4 is obtained from $5.5L_4$ or $5.5L_5$ by connecting a separatrix of the finite saddle with the mentioned transversal orbit. Since the separatrix of the infinite saddle is not a separatrix of the triple node $\overline{\binom{0}{3}}N$, the connection of two orbits in P_4 does not imply a topological change in the phase portrait. See Fig. 16 for an illustration of this fact, where we see that in $5.5L_4$ both finite separatrices arrive to $\overline{\binom{0}{3}}N$ tangentially to the infinity line and in the same direction, in P_4 one separatrix arrives transversally and in $5.5L_5$ it arrives again tangentially to the infinity line but from the opposite direction. Moreover, because of the existence of phase portrait $5.5L_5$, the singular slice $k = 8 - \varepsilon_4^*$ must be considered (and so must P_4), i.e. the red cusp must cross segment $7S_4$.

Finally, it remains to analyze the last singular slice into consideration, $k = k_9 = 0$. For $k = 0$, we

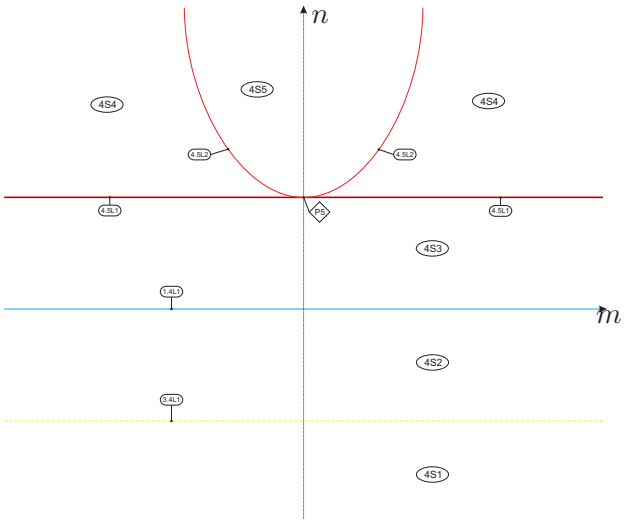

Fig. 17. Slice of parameter space when $k = 0$

calculate:

$$\begin{aligned} &\mu = 4n, \quad \mathcal{T}_4 = -4(n+2), \\ &\eta = 4(m^2+2-n)(n-2)^2, \\ &W_4 = 16(n-2)^2, \quad B_1 = 0. \end{aligned} \tag{21}$$

Then, by Eq. (21), we conclude that surface $(\mathcal{S}_1)$ is the horizontal axis of the slice $k = 0$, surface $(\mathcal{S}_3)$ is the line $n = -2$, surface $(\mathcal{S}_5)$ is the union of the double line $n = 2$ with the parabola $n = m^2+2$ and surface $(\mathcal{S}_6)$ is the double line $n = 2$. We see that surface $(\mathcal{S}_6)$ is part of the surface $(\mathcal{S}_5)$. Moreover, according to Lemma 6.1, since $B_1 = 0$, all the phase portraits in this slice is characterized by having the y–axis as an invariant straight line. Fig. 17 shows the bifurcation diagram for $k = 0$. We note that the labels of slice for $k = 0$ recall surface $(\mathcal{S}_4)$ since all the phase portraits here possess invariant straight line.

Table 5 presents the dead and the born parts in the transition from the generic slice $k = 4$ to the singular slice $k = 0$.

Table 6 shows the correspondent parts when we move from slice $k = 4$ to slice $k = 0$, which makes this transition (or the reversed one) to be coherent. Since there exist coherence between the generic slices bordering the singular slices with their respective generic side slices, no more slices are needed for the complete coherence of the bifurcation diagram.

Table 5. Transition from slice $k = 4$ to $k = 0$

Dead parts	Born parts in Sing. Slice
V_1, V_2, V_3, V_4, V_6, V_8	$4S_1$, $4S_2$, $4S_3$, $4S_4$, $4S_5$
V_{10}, V_{12}, V_{13}, V_{14}, V_{15}	$1.4L_1$, $3.4L_1$, $4.5L_1$
V_{16}, $1S_1$, $1S_2$, $3S_1$, $3S_3$	$4.5L_2$, P_5
$5S_1$, $5S_{10}$, $5S_{11}$, $5S_{12}$	
$5S_{13}$, $6S_1$, $6S_3$, $6S_4$, $7S_1$	
$7S_3$, $1.3L_1$, $5.5L_5$, $5.6L_3$	

Table 6. Coherent correspondence among parts of slice $k = 4$ and parts of slice $k = 0$. The symbol "∞" means that the part for $k = 4$ goes to infinity as $k \to 0$

Parts in $k = 4$	Parts in $k = 0$
V_1	$4S_2$
V_2	$4S_1$
V_3	∞
V_4	∞
V_6	∞
V_8	∞
V_{10}	∞
V_{12}	$4.5L_1$
V_{13}	$4.5L_1$
V_{14}	$4S_4$
V_{15}	$4S_5$
V_{16}	$4S_4$
$1S_1$	$1.4L_1$
$1S_2$	∞
$3S_1$	∞
$3S_3$	$3.4L_1$
$5S_1$	∞
$5S_{10}$	$4.5L_1$
$5S_{11}$	P_5
$5S_{12}$	$4.5L_2$
$5S_{13}$	$4.5L_2$
$6S_1$	∞
$6S_3$	$4.5L_1$
$6S_4$	$4.5L_1$
$7S_1$	∞
$7S_3$	∞
$1.3L_1$	P_5
$5.5L_5$	P_5
$5.6L_3$	P_5

7. Some other relevant facts about the bifurcation diagrams

The bifurcation diagram we have obtained for the family $\mathbf{QT\overline{S}}$ is completely coherent, i.e. by taking any two points in the parameter space and joining them by a continuous curve, along this curve the changes in phase portraits that occur when crossing the different bifurcation surfaces we mention can be completely explained.

However, we cannot be sure that these bifurcation diagrams are the complete bifurcation diagrams for $\mathbf{QT\overline{S}}$ due to the possibility of "islands" inside the parts bordered by unmentioned bifurcation surfaces. In case these "islands" exist, they would not mean any modification of the nature of the singular points. So, on the border of these "islands" we could only have bifurcations due to saddle connections or multiple limit cycles.

In case there were more bifurcation surfaces, we should still be able to join two representatives of any two parts of the 71 parts of $\mathbf{QT\overline{S}}$ found until now with a continuous curve either without crossing such bifurcation surface or, in case the curve crosses it, it must do it an even number of times without tangencies, otherwise one must take into account the multiplicity of the tangency, so the total number must be even. This is why we call these potential bifurcation surfaces "*islands*".

However, we have not found a different phase portrait which could fit in such an island. A potential "island" would be the set of parameters for which the phase portraits possesses a double limit cycle and this "island" would be inside the parts where $W_4 < 0$ since we have the presence of a focus (recall the item (iii) of Sec. 4).

In this case, since the parameter space is not compact, it could even exist new slices for $k > 16$ implying some separatrix connection or double limit cycle. We have tried some bigger values and have not found anything relevant.

8. Completion of the proof of the main theorem

In the bifurcation diagram we may have topologically equivalent phase portraits belonging to distinct parts of the parameter space. As here we have 71 distinct parts of the parameter space, to help us identify or to distinguish phase portraits, we need to introduce some invariants. We consider integer–valued and character invariants. All of them were already used in [Artés *et al.*, 2013], [Artés *et al.*, 2014] and [**?**], but we recall them here. These invariants yield a classification which is easier to grasp.

Definition 8.1. We denote by $I_1(S)$ the number of the real finite singular points.

Definition 8.2. We denote by $I_2(S)$ the sum of the indices of the isolated real finite singular points.

Definition 8.3. We denote by $I_3(S)$ the number of the real infinite singular points.

Definition 8.4. For a given infinite singularity s of a system S, let l_s be the number of global or local separatrices beginning or ending at s and which do not lie on the line at infinity. We have $0 \leq l_s \leq 6$. We denote by $I_4(S)$ the sequence of all such l_s when s moves in the set of infinite singular points of the system S. We start the sequence at the infinite singular point which receives (or sends) the greatest number of separatrices and take the direction which yields the greatest absolute value, e.g. the values 2110 and 2011 for this invariant are symmetrical (and, therefore, they are the same), so we consider 2110.

Definition 8.5. We denote by $I_5(S)$ the number of limit cycles around the focus.

Definition 8.6. We denote by $I_6(S)$ a character from the set $\{n, y\}$ describing the nonexistence ("n") or the existence ("y") of connection of separatrices.

According to Remark 6.21, we do not distinguish between two phase portraits whose only difference is the presence of a finite node instead of a finite focus. Both phase portraits are topologically equivalent and they can only be distinguished within the C^1 class. In case we may want to distinguish them, a new invariant might easily be defined.

Theorem 8.7. *Consider the family* $\mathbf{QT\overline{S}}$ *and all the phase portraits that we have obtained for this family. The values of the affine invariant* $\mathcal{I} = (I_1, I_2, I_3, I_4, I_5, I_6)$ *given in the following diagram*

yield a partition of these phase portraits of the family $\mathbf{QT\overline{S}}$.

Furthermore, for each value of $\mathcal{I}$ *in this diagram there corresponds a single phase portrait; i.e.* S *and* S' *are such that* $I(S) = I(S')$ *if, and only if,* S *and* S' *are topologically equivalent.*

The bifurcation diagram for $\mathbf{QT\overline{S}}$ has 71 parts which produce 27 topologically different phase portraits as described in Table 7. The remaining 44 parts do not produce any new phase portrait which was not included in the 27 previous ones. The difference is basically either the presence of an infinite triple node $\overline{\binom{0}{3}}N$, or the identity under small perturbations.

Regarding the notation in the diagram, the phase portraits having neither limit cycle nor graphic have been denoted surrounded by parenthesis, for example (V_1); the phase portraits having one limit cycle have been denoted surrounded by brackets, for example $[V_8]$; the phase portraits having at least one graphic have been denoted surrounded by curly brackets, for example $\{7S_1\}$.

Proof. The above result follows from the results in the previous sections and a careful analysis of the bifurcation diagrams given in Sec. 6 in Figs. 7 to 17, the definition of the invariants I_j and their explicit values for the corresponding phase portraits. ■

We first make some observations regarding the equivalence relations used in this work: the affine and time rescaling, C^1 and topological equivalences.

The coarsest relation among these three is the topological equivalence and the finest one is the affine equivalence. In fact, we can have two systems which are topologically equivalent but not C^1–equivalent. For example, we could have a system with a finite antisaddle which is a structurally stable node and in another system with a focus, the two systems being topologically equivalent but belonging to distinct C^1–equivalence classes, separated by a surface ($(\mathcal{S}_6)$ in this case) on which the node turns into a focus.

In Table 8 we listed in the first column 27 parts with all the distinct phase portraits of Fig. 1. Corresponding to each part listed in column 1 we have in its horizontal block, all parts whose phase portraits are topologically equivalent to the phase portrait appearing in column 1 of the same horizontal block.

In the second column we have put all the parts whose systems yield topologically equivalent phase portraits to those in the first column but which may have some algebro–geometric features related to the position of the orbits.

In the third (respectively, fourth, and fifth) column we list all parts whose phase portraits have another antisaddle which is a focus (respectively, a node which is at a bifurcation point producing foci close to the node in perturbations, a node–focus to shorten, and a finite weak singular point).

In the last column we list two other reasons for the topological equivalence according to the letter in parenthesis in the index right after the name of the region: (a) presence of invariant straight line; (b) presence of a semi–elemental triple node $\overline{\binom{0}{3}}N$ at infinity.

Whenever phase portraits appear on a horizontal block in a specific column, the listing is done according to the decreasing dimension of the parts where they appear, always placing the lower dimensions on lower lines.

8.1. Proof of the main theorem

The bifurcation diagram described in Sec. 6, plus Table 7 of the geometrical invariants distinguishing the 27 phase portraits, plus Table 8 giving the equivalences with the remaining phase portraits lead to the proof of the main statement of Theorem 1.1.

Table 7. Geometric classification for the family $\mathbf{QT\overline{S}}$

$$
I_1 = \left\{ \begin{array}{l}
1 \;\&\; I_3 = \left\{ \begin{array}{l} 2\ \{1.3L_1\}, \\ 3 \;\&\; I_3 = \left\{ \begin{array}{l} 111010\ (1.4L_1), \\ 211110\ (1S_1), \end{array} \right. \end{array} \right. \\
2 \;\&\; I_2 = \left\{ \begin{array}{l}
-2 \;\&\; I_4 = \left\{ \begin{array}{l} 111111\ (4S_1), \\ 211211\ (V_1), \end{array} \right. \\
0 \;\&\; I_3 = \left\{ \begin{array}{l}
1 \;\&\; I_4 = \left\{ \begin{array}{l} 11\ \{7S_1\}, \\ 21 \;\&\; I_5 = \left\{ \begin{array}{l} 0\ (V_4), \\ 1\ [V_8], \end{array} \right. \end{array} \right. \\
2 \;\&\; I_4 = \left\{ \begin{array}{l} 2110\ (4.5L_1), \\ 2111\ (5.7L_4), \\ 2120\ (5.7L_3), \\ 2211 \;\&\; I_6 = \left\{ \begin{array}{l} n\ (5S_1), \\ y\ \{5.7L_2\}, \end{array} \right. \\ 3120 \;\&\; I_6 = \left\{ \begin{array}{l} n\ (5S_{10}), \\ y\ \{5.7L_1\}, \end{array} \right. \\ 3211 \;\&\; I_5 = \left\{ \begin{array}{l} 0\ (5S_3), \\ 1\ [5S_7], \end{array} \right. \\ 3220\ (5S_8), \\ 4120 \;\&\; I_5 = \left\{ \begin{array}{l} 0\ (5S_2), \\ 1\ [5S_6], \end{array} \right. \end{array} \right. \\
3 \;\&\; I_4 = \left\{ \begin{array}{l} 111010\ (4S_3), \\ 111110\ (7S_4), \\ 211101\ \{7S_2\}, \\ 211110\ (V_3), \\ 221101\ (V_{11}), \\ 311101 \;\&\; I_5 = \left\{ \begin{array}{l} 0\ (V_5), \\ 1\ [V_9]. \end{array} \right. \end{array} \right. \end{array} \right. \end{array} \right.
\end{array} \right.
$$

Table 8. Topological equivalences for the family **QTS̄**

Presented phase portrait	Identical under perturbations	Finite antisaddle focus	Finite antisaddle node–focus	Finite weak point	Other reasons
V_1	V_2			$3S_3$	
V_3	V_{14}, V_{16}	V_{13}	$6S_4$		$4S_4{}^{(a)}$
V_4	V_{10}, V_{12}, V_{15} $7S_3$	V_6	$6S_1$, $6S_3$	$3S_1$	$4S_5{}^{(a)}$ $5.5L_1{}^{(b)}$, $5.5L_2{}^{(b)}$ $5.5L_4{}^{(b)}$, $5.5L_5{}^{(b)}$ $P_1{}^{(b)}$, $P_2{}^{(b)}$, $P_4{}^{(b)}$, $P_5{}^{(b)}$
V_5		V_7	$6S_2$	$3S_2$	
V_8					$5.5L_3{}^{(b)}$
V_9					
V_{11}					
$1S_1$	$1S_2$				
$4S_1$	$4S_2$			$3.4L_1$	
$4S_3$					
$5S_1$	$5S_{12}$, $5S_{13}$	$5S_{11}$	$5.6L_3$		$4.5L_2{}^{(a)}$
$5S_2$		$5S_4$	$5.6L_1$	$3.5L_1$	
$5S_3$		$5S_5$, $5S_9$	$5.6L_2$	$3.5L_2$	
$5S_6$					
$5S_7$					
$5S_8$					
$5S_{10}$					
$7S_1$					$P_3{}^{(b)}$
$7S_2$					
$7S_4$					
$1.3L_1$					
$1.4L_1$					
$4.5L_1$					
$5.7L_1$					
$5.7L_2$					
$5.7L_3$					
$5.7L_4$					

Acknowledgements. The first author is partially supported by a MEC/FEDER grant number MTM 2013–40998–P and by an AGAUR grant number 2014–SGR–568, the second author is is partially supported by CNPq grant "Projeto Universal" 472796/2013-5, by CAPES CSF–PVE–88881.030454/2013–01, by Projeto Temático FAPESP number 2014/00304–2. The first and second authors are partially supported by FP7–PEOPLE–2012–IRSES–316338. The third author is supported by CNPq–PDE 232336/2014–8.

References

Andronov, A.A., Leontovich, E.A., Gordon, I.I. & Maier, A.G. [1973] "Qualitative theory of second–order dynamic systems." *Israel Program for Scientific Translations* (Halsted Press, A division of John Wiley & Sons, NY-Toronto, Ontario).

Artés, J.C., Kooij, R. & Llibre, J. [1998] "Structurally stable quadratic vector fields," Memoires Amer. Math. Soc., **134 (639)**.

Artés, J.C., Llibre, J. & Rezende, A.C. [2016] "Structurally unstable quadratic vector fields of codimension one", *Work in progress.*

Artés, J.C., Llibre, J. & Schlomiuk, D. [2006] "The geometry of quadratic differential systems with a weak focus of second order," *Internat. J. Bifur. Chaos Appl. Sci. Engrg.* **16**, 3127–3194.

Artés, J.C., Llibre, J., Schlomiuk, D. & Vulpe, N.I. [2015a] "From topological to geometric equivalence in the classification of singularities at infinity for quadratic vector fields," *Rocky Mountain J. Math.* **45(1)**, 29–113.

Artés, J.C., Llibre, J. & Vulpe, N. [2008] "Singular points of quadratic systems: a complete classification in the coefficient space $\mathbb{R}^{12}$," *Internat. J. Bifur. Chaos Appl. Sci. Engrg.* **18**, 313–362.

Artés, J.C., Rezende, A.C. & Oliveira, R.D.S. [2013] "Global phase portraits of quadratic polynomial differential systems with a semi–elemental triple node," *Internat. J. Bifur. Chaos Appl. Sci. Engrg.* **23**, 21pp.

Artés, J.C., Rezende, A.C. & Oliveira, R.D.S. [2014] "The geometry of quadratic polynomial differential systems with a finite and an infinite saddle–node (A, B)," *Internat. J. Bifur. Chaos Appl. Sci. Engrg.* **24**, 30pp.

Artés, J.C., Rezende, A.C. & Oliveira, R.D.S. [2015b] "The geometry of quadratic polynomial differential systems with a finite and an infinite saddle–node (C)," *Internat. J. Bifur. Chaos Appl. Sci. Engrg.* **25**, 111pp.

Coppel, W.A. [1966] "A survey of quadratic systems," *J. Differential Equations* **2**, 293–304.

Darboux, G. [1878] "Mémoire sur les équations différentielles algébriques du premier ordre et du premier degré (mélanges)," *Bull. Sci. Math.* **124A**, 60–96, 123–144, 151–200.

Dumortier, F., Llibre, J. & Artés, J.C. [2006] "Qualitative Theory of Planar Differential Systems," *Universitext, Springer–Verlag, New York–Berlin.*

Dumortier, F., Roussarie, R. & Rousseau, C. [1994] "Hilbert's 16th problem for quadratic vector fields," *J. Differential Equations* **110**, 66–133.

Fulton, W. [1969] "Algebraic curves. An introduction to Algebraic Geometry," W.A. Benjamin, Inc, New York.

González, E.A. [1969] "Generic properties of polynomial vector fields at infinity," *Trans. Amer. Math. Soc.* **143**, 201–222.

Hartshorne, R. [1977] "Algebraic geometry," *Graduate Texts in Math.* **52**, Springer.

Hilbert, D. [1900] "Mathematische probleme", *In Nachr. Ges. Wiss., editor Second Internat. Congress Math. Paris, 1900*, 253–297. Göttingen Math.–Phys. Kl.

Hilbert, D. [1902] "Mathematical problems," *Bull. Amer. Math. Soc.* **8**, 437–479.

Llibre, J. & Schlomiuk, D. [2004] "The geometry of quadratic differential systems with a weak focus of third order," *Canad. J. Math.* **56**, 310–343.

Roussarie, R. & Schlomiuk, D. [2002] "On the geometric structure of the class of planar quadratic differential systems," *Qual. Theory Dyn. Syst.* **3**, 93–122.

Schlomiuk, D. & Pal, J. [2001] "On the geometry in the neighborhood of infinity of quadratic differential systems with a weak focus," *Qual. Theory Dyn. Syst.* **2**, 1–43.

Schlomiuk, D. & Vulpe, N.I. [2004] "Planar quadratic differential systems with invariant straight lines of at least five total multiplicity," *Qual. Theory Dyn. Syst.* **5**, 135–194.

Schlomiuk, D. & Vulpe, N.I. [2005] "Geometry of quadratic differential systems in the neighborhood of the infinity," *J. Differential Equations* **215**, 357–400.

Schlomiuk, D. [2014] "Topological and polynomial invariants, moduli spaces in classification problems of polynomial vector fields," *Publ. Mat.* **58**, 461–496.

Vulpe, N.I. [2011] "Characterization of the finite weak singularities of quadratic systems via invariant theory," *Nonlinear Anal.* **74**, 6553–6582.

Ye, Y.Q., Cai, S.L., Chen, L.S., Huang, K.C., Luo, D.J., Ma, Z.E., Wang, E.N., Wang, M.S. & Yang, X.A. [1986] "Theory of limit cycles," *Trans. of Mathematical Monographs*, **66**. Amer. Math. Soc., Providence, RI, 2 edition.